

Machine Intelligence at the Edge with Learning Centric Power Allocation

Shuai Wang, Yik-Chung Wu, Minghua Xia, Rui Wang, and H. Vincent Poor

Abstract

While machine-type communication (MTC) devices generate considerable amounts of data, they often cannot process the data due to limited energy and computation power. To empower MTC with intelligence, edge machine learning has been proposed. However, power allocation in this paradigm requires maximizing the learning performance instead of the communication throughput, for which the celebrated water-filling and max-min fairness algorithms become inefficient. To this end, this paper proposes learning centric power allocation (LCPA), which provides a new perspective to radio resource allocation in learning driven scenarios. By employing an empirical classification error model that is supported by learning theory, the LCPA is formulated as a nonconvex nonsmooth optimization problem, and is solved by majorization minimization (MM) framework. To get deeper insights into LCPA, asymptotic analysis shows that the transmit powers are inversely proportional to the channel gain, and scale exponentially with the learning parameters. This is in contrast to traditional power allocations where quality of wireless channels is the only consideration. Last but not least, to enable LCPA in large-scale settings, two optimization algorithms, termed mirror-prox LCPA and accelerated LCPA, are further proposed. Extensive numerical results demonstrate that the proposed LCPA algorithms outperform traditional power allocation algorithms, and the large-scale algorithms reduce the computation time by orders of magnitude compared with MM-based LCPA but still achieve competing learning performance.

Index Terms

Empirical classification error model, edge machine learning, learning centric communication, multiple-input multiple-output, resource allocation.

S. Wang and R. Wang are with the Department of Electrical and Electronic Engineering, Southern University of Science and Technology, Shenzhen 518055, China (e-mail: {wangs3,wang.r}@sustech.edu.cn). S. Wang has also been with the Department of Electrical and Electronic Engineering, The University of Hong Kong at the time of submission. Y.-C. Wu is with the Department of Electrical and Electronic Engineering, The University of Hong Kong, Hong Kong (e-mail: ycwu@eee.hku.hk). M. Xia is with the School of Electronics and Information Technology, Sun Yat-sen University, Guangzhou, 510006, China (e-mail: xiamingh@mail.sysu.edu.cn). H. V. Poor is with the Department of Electrical Engineering, Princeton University, Princeton, NJ 08544 USA (e-mail: poor@princeton.edu).

I. INTRODUCTION

Machine intelligence is revolutionizing every branch of science and technology [1], [2]. If a machine wants to learn, it requires at least two ingredients: information and computation, which are usually separated from each other in machine-type communication (MTC) systems [3]. Nonetheless, sending vast volumes of data from MTC devices to the cloud not only leads to a heavy communication burden but also increases the transmission latency. To address this challenge brought by MTC, a promising solution is the *edge machine learning* technique [4]–[11] that trains a machine learning model or *fine-tune a pre-trained model* at the edge (i.e., nearby radio access point with computation resources).

In general, there are two ways to implement edge machine learning: data sharing and model sharing. Data sharing uses the edge to collect data generated from MTC devices for machine learning [4]–[7], while model sharing uses federated learning [8]–[11] to exchange model parameters (instead of data) between the edge and users. Both approaches are recognized as key paradigms in the sixth generation (6G) wireless communications [12]–[14]. However, since the MTC devices often cannot process the data due to limited computation power, this paper focuses on data sharing.

A. Motivation and Related Work

In contrast to conventional communication systems, edge machine learning systems aim to maximize the learning performance instead of the communication throughput. Therefore, edge resource allocation becomes very different from traditional resource allocation schemes that merely consider the wireless channel conditions [15]–[18]. For instance, the celebrated water-filling scheme allocates more resources to better channels for throughput maximization [15], and the max-min fairness scheme allocates more resources to cell-edge users to maintain certain quality of service [16]. While these two schemes have proven to be very efficient in traditional wireless communication systems, they could lead to poor learning performance in edge learning systems because they do not account for the machine learning factors such as model and dataset complexities. Imagine training a deep neural network (DNN) and a support vector machine (SVM) at the edge. Due to much larger number of parameters in DNN, the edge should allocate more resources to MTC devices that upload data for the DNN than those for the SVM.

Nonetheless, in order to maximize the learning performance, we need a mathematical expression of the learning performance with respect to the number of samples, which does not

exist to the best of the authors' knowledge. While the sample complexity of a learning task can be related to the Vapnik-Chervonenkis (VC) dimension [1], this theory only provides a vague estimate that is independent of the specific learning algorithm or data distribution. To better understand the learning performance, it has been proved in [19], [20] that the generalization error can be upper bounded by the summation of the bias between the main prediction and the optimal prediction, the variance due to training datasets, and the noise of the target example. With the bound being tight for certain loss functions (e.g., squared loss and zero-one loss), the bias-variance decomposition theory gives rise to an empirical nonlinear classification error model [21]–[23] that is also theoretically supported by the inverse power law derived via statistical mechanics [24].

B. Summary of Results

In this paper, we adopt the above nonlinear model to approximate the learning performance, and a *learning centric power allocation (LCPA)* problem is formulated with the aim of minimizing classification error subject to the total power budget constraint. Since the formulated machine learning resource allocation problem is nonconvex and nonsmooth, it is nontrivial to solve. Despite the two challenges, by leveraging the majorization minimization (MM) framework from optimization, an MM-based LCPA algorithm that converges to a Karush-Kuhn-Tucker (KKT) solution is proposed. To get deeper insights into LCPA, an analytical solution is derived for the asymptotic case, with the number of antennas at the edge going to infinity. The asymptotic optimal solution discloses that the transmit powers are inversely proportional to the channel gain, and scale exponentially with the classification error model parameters. This result reveals that machine learning has a stronger impact than wireless channels in LCPA. To enable affordable computation complexity when the number of MTC devices is extremely large, two variants of LCPA, called mirror-prox LCPA and accelerated LCPA, are proposed. Both algorithms are first-order methods (FOMs), implying that their complexities are linear with respect to the number of users. Furthermore, the iteration complexity for the accelerated LCPA to converge has achieved the lower bound derived for any FOM, meaning that the accelerated LCPA is among the fastest FOMs for solving the considered problem. Extensive experimental results based on public datasets show that the proposed LCPA scheme is able to achieve a higher classification accuracy than that of the sum-rate maximization and max-min fairness power allocation schemes. For the first time, the benefit brought by joint communication and learning design is quantitatively

demonstrated in edge machine learning systems. Our results also show that both the mirror-prox LCPA and accelerated LCPA reduce the computation time by orders of magnitude compared to the MM-based LCPA but still achieve satisfactory performance.

To sum up, the contributions of this paper are listed as follows.

- A learning centric power allocation (LCPA) scheme is developed for the edge machine learning problem, which maximizes the learning accuracy instead of the communication throughput.
- To understand how LCPA works, an asymptotic optimal solution to the edge machine learning problem is derived, which, for the first time, discloses that the transmit power obtained from LCPA grows linearly with the path loss and grows exponentially with the learning parameters.
- To reduce the computation time of LCPA in the massive multiple-input multiple-output (MIMO) setting, two variants of LCPA based on FOMs are proposed, which enable the edge machine learning system to scale up the number of MTC users.
- Extensive experimental results based on public datasets (e.g., MNIST, CIFAR-10, ModelNet40) show that the proposed LCPA is able to achieve a higher accuracy than that of the sum-rate maximization and max-min fairness schemes.

C. Outline

The rest of this paper is organized as follows. System model and problem formulation are described in Section II. Classification error modeling is presented in Section III. The MM-based LCPA algorithm, and asymptotic solutions are derived in Sections IV and V, respectively. Finally, experimental results are presented in Section VI, and conclusions are drawn in Section VII.

Notation: Italic letters, lowercase and uppercase bold letters represent scalars, vectors, and matrices, respectively. Curlicue letters stand for sets and $|\cdot|$ is the cardinality of a set. The operators $(\cdot)^T$, $(\cdot)^H$ and $(\cdot)^{-1}$ take the transpose, Hermitian and inverse of a matrix, respectively. We use (a_1, a_2, \dots) to represent a sequence, $[a_1, a_2, \dots]^T$ to represent a column vector, and $\|\cdot\|_p$ to represent the ℓ_p -norm of a vector. The symbol \mathbf{I}_N indicates the $N \times N$ identity matrix, $\mathbf{1}_N$ indicates the $N \times 1$ vector with all entries being one, and $\mathcal{CN}(0, 1)$ stands for complex Gaussian distribution with zero mean and unit variance. The function $[x]^+ = \max(x, 0)$, while $\exp(\cdot)$ and $\ln(\cdot)$ denote the exponential function and the logarithm function, respectively. Finally, $\mathbb{E}(\cdot)$ means the expectation of a random variable, $\mathbb{I}_{\mathcal{A}}(x) = 1$ if $x \in \mathcal{A}$ and zero otherwise, and $\mathcal{O}(\cdot)$

TABLE I
SUMMARY OF IMPORTANT VARIABLES AND PARAMETERS

Symbol	Type	Description
$p_k \in \mathbb{R}_+$	Variable	Transmit power (in Watt) at user k .
$v_m \in \mathbb{Z}_+$	Variable	Number of training samples for task m .
P	Parameter	Total transmit power budget (in Watt).
B	Parameter	Communication bandwidth (in Hz).
T	Parameter	Transmission time (in s) of the data collection.
D_m	Parameter	Data size (in bit) per sample for task m .
A_m	Parameter	Initial number of samples at the edge for task m .
σ^2	Parameter	Noise power (in Watt).
$G_{k,l}$	Parameter	The composite channel gain from user l to the edge when detecting data of user k .
$\Psi_m(v_m)$	Function	Classification error of the learning model m when the sample size is v_m .
$\Theta_m(v_m a_m, b_m)$	Function	Empirical classification error model for task m with parameters (a_m, b_m) .

means the order of arithmetic operations. Important variables and parameters to be used in this paper are listed in Table I.

II. SYSTEM MODEL AND PROBLEM FORMULATION

We consider an edge machine learning system shown in Fig. 1, which consists of an intelligent edge with N antennas and K users. The goal of the edge is to train M classification models by collecting data observed at M user groups¹ (e.g., UAVs with camera sensors) $\{\mathcal{Y}_1, \mathcal{Y}_2, \dots, \mathcal{Y}_M\}$, with the group \mathcal{Y}_m storing the data for training the model m . For the classification models, without loss of generality, Fig. 1 depicts a convolutional neural network (CNN) and a support vector machine (SVM) with $M = 2$, but more user groups and other classification models are equally valid. It is assumed that the data are labeled at the edge. This can be supplemented by the recent self-labeled techniques [25], [26], where a classifier is trained with an initial small number of labeled examples, and then the model is retrained with its own most confident predictions, thus enlarging its labeled training set. After training the classifiers, the edge can feedback the trained models to users for subsequent use (e.g., object recognition). Notice that if the classifiers are pre-trained at the cloud and deployed at the edge, the task of edge machine learning is to fine-

¹In case where some data from a particular user is used to train both model m and model j , we can allow \mathcal{Y}_m and \mathcal{Y}_j to include a common user. That is, $\mathcal{Y}_m \cap \mathcal{Y}_j \neq \emptyset$ for $m \neq j$.

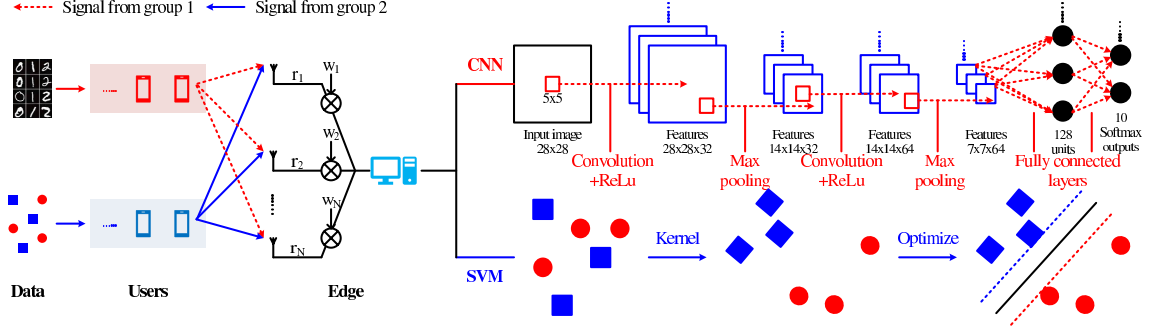


Fig. 1. System model of machine learning at the edge.

tune the pre-trained models at the edge, using local data generated from MTC users. Based on the above description, the edge needs to collect the data and learn from them.

More specifically, the user $k \in \{1, \dots, K\}$ transmits a signal s_k with power $\mathbb{E}[|s_k|^2] = p_k$. Accordingly, the received signal $\mathbf{r} = [r_1, \dots, r_N]^T \in \mathbb{C}^{N \times 1}$ at the edge is $\mathbf{r} = \sum_{k=1}^K \mathbf{h}_k s_k + \mathbf{n}$, where $\mathbf{h}_k \in \mathbb{C}^{N \times 1}$ is the channel vector from the k^{th} user to the edge, and $\mathbf{n} \sim \mathcal{CN}(\mathbf{0}, \sigma^2 \mathbf{I}_N)$. By applying the well-known maximal ratio combining (MRC) receiver $\mathbf{w}_k = \mathbf{h}_k / \|\mathbf{h}_k\|_2$ to \mathbf{r} , the data-rate of user k is

$$R_k = \log_2 \left(1 + \frac{G_{k,k} p_k}{\sum_{l=1, l \neq k}^K G_{k,l} p_l + \sigma^2} \right), \quad (1)$$

where $G_{k,l}$ represents the composite channel gain (including channel fading and MIMO processing) from user l to the edge when detecting data of user k :

$$G_{k,l} = \begin{cases} \|\mathbf{h}_k\|_2^2, & \text{if } k = l \\ \frac{|\mathbf{h}_k^H \mathbf{h}_l|^2}{\|\mathbf{h}_k\|_2^2}, & \text{if } k \neq l \end{cases}. \quad (2)$$

With the expression of R_k in (1), the amount of data in bit received from user k is BTR_k , where constant B is the bandwidth in Hz that is assigned to the system (e.g., a standard MTC system would have 180 kHz bandwidth [27]), and T is the total number of transmission time in second. As a result, the total number of training samples that are collected at the edge for training the model m is

$$v_m = \sum_{k \in \mathcal{Y}_m} \left\lfloor \frac{BTR_k}{D_m} \right\rfloor + A_m \approx \sum_{k \in \mathcal{Y}_m} \frac{BTR_k}{D_m} + A_m, \quad (3)$$

where A_m is the initial number of samples for task m at the edge, $\lfloor x \rfloor = \max\{n \in \mathbb{Z} : n \leq x\}$ and the approximation is due to $\lfloor x \rfloor \rightarrow x$ when $x \gg 1$. Notice that D_m is the number of bits for

each data sample. For example, the handwritten digits in the MNIST dataset [28] are grayscale images with 28×28 pixels (each pixel has 8 bits), and in this case $D_m = 8 \times 28 \times 28 + 4 = 6276$ bits (4 bits are reserved for the labels of 10 classes [28] in case the users also transmit labels). With the collected samples, the intelligent edge can train models $m = 1, \dots, M$ in the learning phase.

In the considered system, the design variables that can be controlled are the transmit powers of different users $\mathbf{p} = [p_1, \dots, p_K]^T$ and the sample sizes of different models $\mathbf{v} = [v_1, \dots, v_M]^T$. Since the power costs at users should not exceed the total budget P , the variable \mathbf{p} needs to satisfy $\sum_{k=1}^K p_k = P$. Having the transmit power satisfied, it is then crucial to minimize the classification errors (i.e., the number of incorrect predictions divided by the number of total predictions), which leads to the following learning centric power allocation (LCPA) problem:

$$\begin{aligned} \text{P : } & \min_{\mathbf{p}, \mathbf{v}} \quad \max_{m=1, \dots, M} \quad \Psi_m(v_m), \\ & \text{s.t.} \quad \sum_{k=1}^K p_k = P, \quad p_k \geq 0, \quad \forall k = 1, \dots, K, \end{aligned} \quad (4a)$$

$$\sum_{k \in \mathcal{Y}_m} \frac{BT}{D_m} \log_2 \left(1 + \frac{G_{k,k} p_k}{\sum_{l=1, l \neq k}^K G_{k,l} p_l + \sigma^2} \right) + A_m = v_m, \quad \forall m = 1, \dots, M, \quad (4b)$$

where $\Psi_m(v_m)$ is the classification error of the learning model m when the sample size is v_m , and the min-max operation at the objective function is to guarantee the worst-case learning performance. The key challenge to solve P is that functions (Ψ_1, \dots, Ψ_M) represent generalization errors, and to the best of the authors' knowledge, currently there is no exact expression of $\Psi_m(v_m)$. To address this issue, the following section will adopt an empirical classification error model to approximate Ψ_m .

Remark: When data is non-uniformly distributed among users, the learning error would likely depend on how much data each user could contribute to the learning task. In this case, the proposed method can still be applied by adding constraints

$$\frac{BT}{D_m} \log_2 \left(1 + \frac{G_{k,k} p_k}{\sum_{l=1, l \neq k}^K G_{k,l} p_l + \sigma^2} \right) \leq Z_k, \quad \forall k = 1, \dots, K \quad (5)$$

to P, where Z_k is the maximum number of samples to be collected from user k . For example, if the data from user k is not important or there is not enough data at user k , we can set a small Z_k .

III. MODELING OF CLASSIFICATION ERROR

In general, the classification error $\Psi_m(v_m)$ is a nonlinear function of v_m [19]–[24]. Particularly, this nonlinear function should satisfy the following properties:

- (i) Since Ψ_m is a percentage, it is bounded as $0 \leq \Psi_m(v_m) \leq 1$;
- (ii) Since more data would provide more information, $\Psi_m(v_m)$ is a monotonically decreasing function of v_m [21];
- (iii) As v_m increases, the magnitude of derivative $|\partial\Psi_m/\partial v_m|$ would gradually decrease and become zero when v_m is sufficiently large [22], meaning that increasing sample size no longer helps machine learning.

Based on the properties (i)–(iii), the following nonlinear model $\Theta_m(v_m|a_m, b_m)$ [21]–[23] can be used to capture the shape of $\Psi_m(v_m)$:

$$\Psi_m(v_m) \approx \Theta_m(v_m|a_m, b_m) = a_m \times v_m^{-b_m}, \quad (6)$$

where $a_m, b_m \geq 0$ are tuning parameters. It can be seen that Θ_m satisfies all the features (i)–(iii). Moreover, $\Theta_m(v_m|a_m, b_m) \rightarrow 0$ if $v_m \rightarrow +\infty$, meaning that the error is 0 with infinite data².

Interpretation from Learning Theory. Apart from (i)–(iii), the model (6) corroborates the *inverse power relationship* between learning performance Ψ_m and the amount of training data v_m from the perspective of statistical mechanics [24]. The error model in (6) can also be explained by the bias-variance decomposition theory [19], [20]. In particular, it is known that the probability of incorrect classification is proportional to the summation of a bias term and a variance term [19]. The bias is independent of the training set, and is zero for a learner that always makes the optimal prediction [20]. The variance is independent of the true value of the predicted variable, and is asymptotically proportional to $1/v_m$ for independent and identically distributed (IID) samples [21]. But since the datasets could be finite and non-IID, we use $v_m^{-b_m}$ to represent the error rate, with b_m being a tuning parameter to account for the *non-IID dataset*. Finally, by multiplying a weighting factor a_m to account for the *model complexity* of the classifier m , we immediately obtain the result in (6).

A. Parameter Fitting of CNN and SVM Classifiers

We use the public MNIST dataset [28] as the input images, and train the 6-layer CCN (shown in Fig. 1) with training sample size $v_m^{(i)}$ ranging from 100 to 10000. In particular, the input image

²We assume the model is powerful enough such that given infinite amount of data, the error rate can be driven to zero.

is sequentially fed into a 5×5 convolution layer (with ReLu activation, 32 channels, and SAME padding), a 2×2 max pooling layer, then another 5×5 convolution layer (with ReLu activation, 64 channels, and SAME padding), a 2×2 max pooling layer, a fully connected layer with 128 units (with ReLu activation), and a final softmax output layer (with 10 outputs). The training procedure is implemented via Adam optimizer with a learning rate of 10^{-4} and a mini-batch size of 100. After training for 5000 iterations, we test the trained model on a validation dataset with 1000 unseen samples, and compute the corresponding classification error. By varying the sample size v_m as $(v_m^{(1)}, v_m^{(2)}, \dots) = (100, 150, 200, 300, 500, 1000, 5000, 10000)$, we can obtain the classification error $\Psi_m(v_m^{(i)})$ for each sample size $v_m^{(i)}$, where $i = 1, \dots, Q$, and $Q = 8$ is the number of points to be fitted. With $\{v_m^{(i)}, \Psi_m(v_m^{(i)})\}_{i=1}^Q$, the parameters (a_m, b_m) in Θ_m can be found via the following nonlinear least squares fitting:

$$\min_{a_m, b_m} \frac{1}{Q} \sum_{i=1}^Q \left| \Psi_m(v_m^{(i)}) - \Theta_m(v_m^{(i)} | a_m, b_m) \right|^2, \quad \text{s.t.} \quad a_m \geq 0, \quad b_m \geq 0. \quad (7)$$

The above problem can be solved by two-dimensional brute-force search, or gradient descent method. Since the parameters (a_m, b_m) for different tasks are obtained independently, the total complexity is linear in terms of the number of tasks.

To demonstrate the versatility of the model, we also fit the nonlinear model to the classification error of a support vector machine (SVM) classifier. The SVM uses penalty coefficient $C = 1$ and Gaussian kernel function $K(\mathbf{x}_i, \mathbf{x}_j) = \exp(-\tilde{\gamma} \times \|\mathbf{x}_i - \mathbf{x}_j\|_2^2)$ with $\tilde{\gamma} = 0.001$ [29]. Moreover, the SVM classifier is trained on the digits dataset in the Scikit-learn Python machine learning toolbox, and the dataset contains 1797 images of size 8×8 from 10 classes, with 5 bits (corresponding to integers 0 to 16) for each pixel [29]. Therefore, each image needs $D_m = 8 \times 8 \times 5 + 4 = 324$ bits. Out of all images, we train the SVM using the first 1000 samples with sample size $(v_m^{(1)}, v_m^{(2)}, \dots) = (30, 50, 100, 200, 300, 400, 500, 1000)$, and use the latter 797 samples for testing. The parameters (a_m, b_m) for the SVM are obtained following a similar procedure in (7).

The fitted classification error versus the sample size is shown in Fig. 2a. It is observed from Fig. 2a that with the parameters $(a_m, b_m) = (9.27, 0.74)$, the nonlinear classification error model in (6) matches the experimental data of CNN very well. Furthermore, with $(a_m, b_m) = (6.94, 0.8)$, the model in (6) fits the experimental data of SVM.

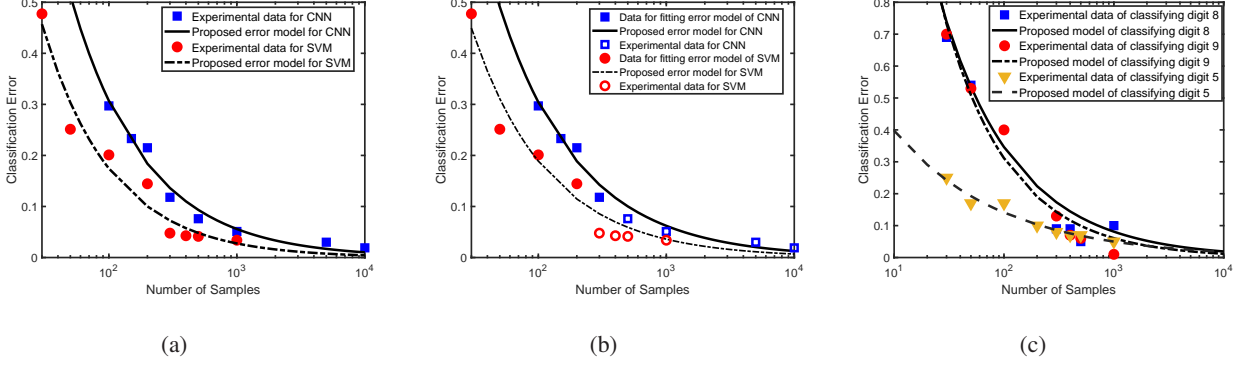


Fig. 2. a) Comparison between the experimental data and the nonlinear classification error model. The parameters in the models are given by $(a_m, b_m) = (9.27, 0.74)$ for CNN and $(a_m, b_m) = (6.94, 0.8)$ for SVM; b) Fitting the error function to small datasets. The parameters in the models are given by $(a_m, b_m) = (7.3, 0.69)$ for CNN and $(a_m, b_m) = (5.2, 0.72)$ for SVM; c) Comparison between different classification tasks.

B. Practical Implementation

One may wonder how could one obtain the fitted classification error model before the actual machine learning model is being trained. There are two ways to address this issue.

1) Extrapolation. More specifically, the error function can be obtained by training the machine learning model on an initial dataset (i.e., with a maximum size of A_m) at the edge, and the performance on a future larger dataset can be predicted. This is called extrapolation [21]. For example, by fitting the error function to the first half experimental data of CNN in Fig. 2b (i.e., $v_m = (100, 150, 200, 300)$), we can obtain $(a_m, b_m) = (7.3, 0.69)$, and the resultant curve predicts the errors at $v_m = (500, 1000, 5000, 10000)$ very well as shown in Fig. 2b. Similarly, with $(a_m, b_m) = (5.2, 0.72)$ obtained from the experimental data of $v_m = (30, 50, 100, 200)$, the proposed model for SVM matches the classification errors at $v_m = (300, 400, 500, 1000)$. It can be seen that the fitting performance in Fig. 2b is slightly worse than that in Fig. 2a, as we use smaller number of pilot data. But since our goal is to distinguish different tasks rather than accurate prediction of the classification errors, such an extrapolation method can still guide the resource allocation at the edge.

2) Approximation. This means that we can pre-train a large number of commonly-used models offline (not at the edge) and store their corresponding parameters of (a_m, b_m) in a look-up table at the edge. Then by choosing a set of parameters from the table, the unknown error model at the edge can be approximated. This is because the error functions can share the same trend for two similar tasks, e.g., classifying digit ‘8’ and ‘9’ with SVM as shown in Fig. 2c. Notice that

there may be a mismatch between the pre-training task and the real task at the edge. This is the case between classifying digit ‘8’ and ‘5’ in Fig. 2c. As a result, it is necessary to carefully measure the similarity between two tasks before choosing the parameters.

IV. MM-BASED LCPA ALGORITHM

Based on the results in Section III, we can directly approximate the true error function Ψ_m by Θ_m . However, to account for the approximation error between Ψ_m and Θ_m (e.g., due to noise in samples or slight mismatch between data used for training and data observed in MTC devices), a weighting factor $\beta_m \geq 1$ can be applied to Θ_m , where a higher value of β_m accounts for a larger approximation error. Then by replacing Ψ_m with $\beta_m \Theta_m$ and putting (4b) into $\Theta_m(v_m|a_m, b_m)$ to eliminate \mathbf{v} , problem P becomes:

$$\begin{aligned} \text{P1 : } \min_{\mathbf{p}} \quad & \max_{m=1, \dots, M} \beta_m \times \Phi_m(\mathbf{p}), \\ \text{s.t.} \quad & \sum_{k=1}^K p_k = P, \quad p_k \geq 0, \quad \forall k = 1, \dots, K, \end{aligned} \quad (8)$$

where

$$\Phi_m(\mathbf{p}) := a_m \left[\sum_{k \in \mathcal{Y}_m} \frac{BT}{D_m} \log_2 \left(1 + \frac{G_{k,k} p_k}{\sum_{l=1, l \neq k}^K G_{k,l} p_l + \sigma^2} \right) + A_m \right]^{-b_m}. \quad (9)$$

It can be seen that P1 is a nonlinear optimization problem due to the nonlinear classification error model (6). Moreover, the min operator introduces non-smoothness to the problem, and the objective function is not differentiable. As a result, existing methods based on gradient descent [18] are not applicable.

To solve P1, we propose to use the framework of MM [30]–[33], which constructs a sequence of upper bounds $\{\tilde{\Phi}_m\}$ on $\{\Phi_m\}$ and replaces $\{\Phi_m\}$ in (8) with $\{\tilde{\Phi}_m\}$ to obtain the surrogate problems. More specifically, given any feasible solution \mathbf{p}^* to P1, we define surrogate functions

$$\begin{aligned} \tilde{\Phi}_m(\mathbf{p}|\mathbf{p}^*) = a_m \left\{ \sum_{k \in \mathcal{Y}_m} \frac{BT}{D_m \ln 2} \left[\ln \left(\sum_{l=1}^K \frac{G_{k,l} p_l}{\sigma^2} + 1 \right) - \ln \left(\sum_{l=1, l \neq k}^K \frac{G_{k,l} p_l^*}{\sigma^2} + 1 \right) \right. \right. \\ \left. \left. - \left(\sum_{l=1, l \neq k}^K \frac{G_{k,l} p_l^*}{\sigma^2} + 1 \right)^{-1} \left(\sum_{l=1, l \neq k}^K \frac{G_{k,l} p_l}{\sigma^2} + 1 \right) + 1 \right] + A_m \right\}^{-b_m}, \end{aligned} \quad (10)$$

and the following proposition can be established.

Proposition 1. *The functions $\{\tilde{\Phi}_m\}$ satisfy the following conditions:*

- (i) *Upper bound condition:* $\tilde{\Phi}_m(\mathbf{p}|\mathbf{p}^*) \geq \Phi_m(\mathbf{p})$.
- (ii) *Convexity:* $\tilde{\Phi}_m(\mathbf{p}|\mathbf{p}^*)$ is convex in \mathbf{p} .
- (iii) *Local condition:* $\tilde{\Phi}_m(\mathbf{p}^*|\mathbf{p}^*) = \Phi_m(\mathbf{p}^*)$ and $\nabla_{\mathbf{p}}\tilde{\Phi}_m(\mathbf{p}^*|\mathbf{p}^*) = \nabla_{\mathbf{p}}\Phi_m(\mathbf{p}^*)$.

Proof. See Appendix A. ■

With part (i) of **Proposition 1**, an upper bound can be directly obtained if we replace the functions $\{\Phi_m\}$ by $\tilde{\Phi}_m$ around a feasible point. However, a tighter upper bound can be achieved if we treat the obtained solution as another feasible point and continue to construct the next-round surrogate function. In particular, assuming that the solution at the n^{th} iteration is given by $\mathbf{p}^{[n]}$, the following problem is considered at the $(n+1)^{\text{th}}$ iteration:

$$\begin{aligned} \text{P1}[n+1] : \min_{\mathbf{p}} \quad & \max_{m=1, \dots, M} \beta_m \tilde{\Phi}_m(\mathbf{p}|\mathbf{p}^{[n]}) \\ \text{s.t.} \quad & \sum_{k=1}^K p_k = P, \quad p_k \geq 0, \quad \forall k = 1, \dots, K. \end{aligned} \quad (11)$$

Based on part (ii) of **Proposition 1**, the problem P1[$n+1$] is convex and can be solved by off-the-shelf software packages (e.g., CVX Mosek [34]) for convex programming. Denoting its optimal solution as \mathbf{p}^* , we can set $\mathbf{p}^{[n+1]} = \mathbf{p}^*$, and the process repeats with solving the problem P1[$n+2$]. According to part (iii) of **Proposition 1** and [30, Theorem 1], the sequence $(\mathbf{p}^{[0]}, \mathbf{p}^{[1]}, \dots)$ converges to the KKT solution to P1 for any feasible starting point $\mathbf{p}^{[0]}$ (e.g., $\mathbf{p}^{[0]} = P/K \mathbf{1}_K$). The entire procedure of MM-based LCPA is summarized in Fig. 3.

In terms of computational complexity, P1[$n+1$] involves K primal variables and $M+K+1$ dual variables³. Therefore, the worst-case complexity for solving P1[$n+1$] is $\mathcal{O}\left((M+2K+1)^{3.5}\right)$ [35]. Consequently, the total complexity for solving P1 is $\mathcal{O}\left(\text{Iter}(M+2K+1)^{3.5}\right)$, where Iter is the number of iterations needed for the algorithm to converge.

V. ASYMPTOTIC OPTIMAL SOLUTION TO P1

Although a KKT solution to P1 has been derived in Section IV, it can be seen that MM-based LCPA requires a cubic complexity with respect to K . This leads to time-consuming computations if K is in the range of hundreds or more. As a result, low-complexity large-scale optimization algorithms are indispensable. To this end, in this section we investigate the asymptotic case when

³The dual variables correspond to $M+K+1$ constraints in P1[$n+1$], where M constraints come from the operator $\min_{m=1, \dots, M}$, K constraints come from nonnegative power constraints, and 1 constraint comes from the power budget.

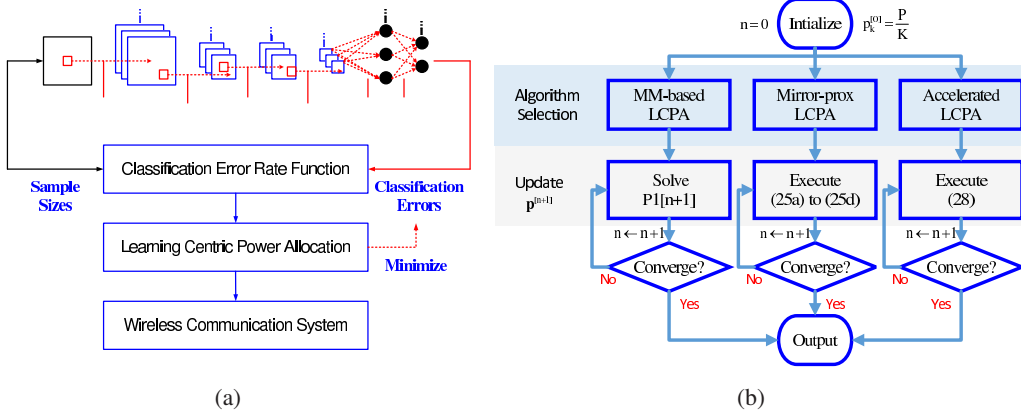


Fig. 3. a) The architecture of edge learning with LCPA; b) The flowchart for LCPA Algorithms.

the number of antennas at the edge approaches infinite (i.e., $N \rightarrow +\infty$), which can facilitate the algorithm design via the law of large numbers [36]–[38].

As $N \rightarrow +\infty$, the channels from different users to the edge would be asymptotically orthogonal [37] and we have

$$G_{k,l} = \frac{|\mathbf{h}_k^H \mathbf{h}_l|^2}{\|\mathbf{h}_k\|_2^2} \rightarrow 0, \quad \forall k \neq l. \quad (12)$$

Based on such orthogonality feature, and putting $G_{k,l} = 0$ for $k \neq l$ into Φ_m in P1, the function Φ_m is asymptotically equal to

$$\Xi_m(\mathbf{p}) = a_m \left[\sum_{k \in \mathcal{Y}_m} \frac{BT}{D_m} \log_2 \left(1 + \frac{G_{k,k} p_k}{\sigma^2} \right) + A_m \right]^{-b_m}. \quad (13)$$

Therefore, the problem P1 when $N \rightarrow +\infty$ is equivalent to

$$\begin{aligned} \text{P2 : } \min_{\mathbf{p}} \quad & \max_{m=1, \dots, M} \beta_m \Xi_m(\mathbf{p}) \\ \text{s.t.} \quad & \sum_{k=1}^K p_k = P, \quad p_k \geq 0, \quad \forall k = 1, \dots, K. \end{aligned} \quad (14)$$

Now it can be seen that by adopting the asymptotic analysis, the function Ξ_m in (13) is much simpler than Φ_m in P1. However, the summation $\sum_{k \in \mathcal{Y}_m}$ in the base of the power function in (13) still hinders us from computing the solution of \mathbf{p} . To address this challenge, the following subsection will derive the closed-form solution to P2 for the special case of $|\mathcal{Y}_m| = 1$ for all m . Then we step further to tackle the general case of $|\mathcal{Y}_m| > 1$ in Section V-B. Finally, an acceleration scheme to achieve faster convergence is discussed in Section V-C.

A. Analytical LCPA When $|\mathcal{Y}_m| = 1$

When $|\mathcal{Y}_m| = 1$ (i.e., each user group has only one user), the summation $\sum_{k \in \mathcal{Y}_m}$ can be dropped and we have $M = K$. For notational simplicity, we denote the unique user in group \mathcal{Y}_m as user $m = k$. Then problem P2 in (14) is rewritten as

$$\begin{aligned} \text{P3: } \min_{\mathbf{p}, \mu} \quad & \mu, \\ \text{s.t.} \quad & \beta_k a_k \left(\frac{BT}{D_k} \log_2 \left(1 + \frac{G_{k,k} p_k}{\sigma^2} \right) + A_k \right)^{-b_k} \leq \mu, \quad \forall k = 1, \dots, K, \end{aligned} \quad (15a)$$

$$\sum_{k=1}^K p_k = P, \quad p_k \geq 0, \quad \forall k = 1, \dots, K, \quad (15b)$$

where $\mu \in [0, 1]$ is a slack variable and has the interpretation of *classification error level*, and the following proposition gives the optimal solution to P3.

Proposition 2. *The optimal \mathbf{p}^* to P3 is*

$$p_k^*(\mu) = \left[\frac{\sigma^2}{G_{k,k}} \exp \left(\frac{D_k \ln 2}{BT} \left[\left(\frac{\mu}{\beta_k a_k} \right)^{-1/b_k} - A_k \right] \right) - \frac{\sigma^2}{G_{k,k}} \right]^+, \quad k = 1, \dots, K, \quad (16)$$

where μ satisfies $\sum_{k=1}^K p_k^*(\mu) = P$.

Proof. See Appendix B. ■

To efficiently compute the classification error level μ , it is observed that the function $p_k^*(\mu)$ is a decreasing function of μ . Therefore, the classification error level μ can be obtained from solving $\sum_{k=1}^K p_k^*(\mu) = P$ using bisection method within interval $[0, 1]$. More specifically, given μ_{\max} and μ_{\min} (initially $\mu_{\max} = 1$ and $\mu_{\min} = 0$), we set $\mu = (\mu_{\max} + \mu_{\min})/2$. If $\sum_k p_k^*(\mu) \geq P$, we update $\mu_{\min} = \mu$; otherwise, we update $\mu_{\max} = \mu$. This procedure is repeated until $|\mu_{\max} - \mu_{\min}| < \epsilon$ with $\epsilon = 10^{-8}$. Since bisection method has a linear convergence rate [39], and in each iteration we need to compute K scalar functions $p_1^*(\mu), \dots, p_K^*(\mu)$, the bisection method has a complexity of $\mathcal{O}(\log(\frac{1}{\epsilon}) K)$.

Scaling Law of Learning Centric Communication. According to **Proposition 2**, the user transmit power p_k is inversely proportional to the wireless channel gain $G_{k,k} = \|\mathbf{h}_k\|_2^2$. However, it is exponentially dependent on the classification error level μ and the learning parameters (a_k, b_k, D_k, A_k) . Moreover, among all parameters, b_k is the most important factor, since b_k is involved in both the power and exponential functions. The above observations disclose that in edge machine learning systems, the learning parameters will have more significant impacts on

the physical-layer design than those of the wireless channels. This result is a joint effect of the Shannon information theory and the learning theory.

Learning Centric versus Communication Centric Power Allocation. Notice that the result in (16) is fundamentally different from the most well-known resource allocation schemes (e.g., iterative water-filling [15] and max-min fairness [16]). For example, the water-filling solution for maximizing the system throughput under $N \rightarrow +\infty$ is given by

$$p_k^{\text{WF}} = \left(\frac{1}{\lambda \ln 2} - \frac{\sigma^2}{G_{k,k}} \right)^+, \quad (17)$$

where λ is a constant chosen such that $\sum_{k=1}^K p_k^{\text{WF}} = P$. On the other hand, the max-min fairness solution under $N \rightarrow +\infty$ is given by

$$p_k^{\text{FAIR}} = P \left(\sum_{k=1}^K \frac{\sigma^2}{G_{k,k}} \right)^{-1} \frac{\sigma^2}{G_{k,k}}. \quad (18)$$

It can be seen from (17) and (18) that the water-filling scheme would allocate more power resources to better channels, and the max-min fairness scheme would allocate more power resources to worse channels. But no matter which scheme we adopt, the only impact factor is the channel condition $\sigma^2/G_{k,k}$.

B. Mirror-Prox LCPA When $|\mathcal{Y}_m| > 1$

In the last subsection, we have derived the closed-form solution to P2 when $|\mathcal{Y}_m| = 1$. However, if the number of users $|\mathcal{Y}_m|$ in each group is larger than 1, the operator $\sum_{k \in \mathcal{Y}_m}$ in (13) cannot be dropped, and there is no closed-form solution to P2. In this general setting, the major challenge comes from the nonsmooth operator min in the objective function, which hinders us from computing the gradients.

To deal with the non-smoothness, we reformulate P2 into a smooth bilevel optimization problem with ℓ_1 -norm (simplex) constraints. Observing that the projection onto a simplex in Euclidean space requires high computational complexities, a mirror-prox LCPA method working on non-Euclidean manifold is proposed. In this way, the distance is measured by Kullback-Leibler (KL) divergence, and the non-Euclidean projection would have analytical expressions. Lastly, with an extragradient step, the proposed mirror-prox LCPA converges to the global optimal solution to P2 with an iteration complexity of $\mathcal{O}(1/\epsilon)$ [40]–[42], where ϵ is the target solution accuracy.

More specifically, we first equivalently transform P2 into a smooth bilevel optimization problem. By defining set $\mathcal{P} = \{\mathbf{p} \in \mathbb{R}_+^{K \times 1} : \|\mathbf{p}\|_1 = P\}$ and introducing variables $\boldsymbol{\alpha} \in \mathbb{R}^{M \times 1}$ such that $\boldsymbol{\alpha} \in \mathcal{A} = \{\boldsymbol{\alpha} \in \mathbb{R}_+^{M \times 1} : \|\boldsymbol{\alpha}\|_1 = 1\}$, P2 is rewritten as

$$\text{P4} : \min_{\mathbf{p} \in \mathcal{P}} \max_{\boldsymbol{\alpha} \in \mathcal{A}} \underbrace{\sum_{m=1}^M \alpha_m \times \beta_m \Xi_m(\mathbf{p})}_{\Upsilon(\boldsymbol{\alpha}, \mathbf{p})}. \quad (19)$$

It can be seen from P4 that $\Upsilon(\boldsymbol{\alpha}, \mathbf{p})$ is differentiable with respect to either \mathbf{p} or $\boldsymbol{\alpha}$, and the corresponding gradients are

$$\nabla_{\mathbf{p}} \Upsilon(\boldsymbol{\alpha}, \mathbf{p}) = \sum_{m=1}^M \alpha_m \beta_m \nabla_{\mathbf{p}} \Xi_m(\mathbf{p}), \quad (20a)$$

$$\nabla_{\boldsymbol{\alpha}} \Upsilon(\boldsymbol{\alpha}, \mathbf{p}) = [\beta_1 \Xi_1(\mathbf{p}), \dots, \beta_M \Xi_M(\mathbf{p})]^T, \quad (20b)$$

where

$$\nabla_{\mathbf{p}} \Xi_m(\mathbf{p}) = \left[\frac{\partial \Xi_m}{\partial p_1}, \dots, \frac{\partial \Xi_m}{\partial p_K} \right]^T, \quad (21)$$

with its j^{th} element being

$$\frac{\partial \Xi_m}{\partial p_j} = -a_m b_m \left[\sum_{k \in \mathcal{Y}_m} \frac{BT}{D_m} \log_2 \left(1 + \frac{G_{k,k} p_k}{\sigma^2} \right) + A_m \right]^{-b_m - 1} \times \frac{BT \mathbb{I}_{\mathcal{Y}_m}(j)}{D_m \ln 2 (\sigma^2 G_{j,j}^{-1} + p_j)}. \quad (22)$$

However, P4 is a bilevel problem, with both the upper layer variable \mathbf{p} and the lower layer variable $\boldsymbol{\alpha}$ involved in the simplex constraints. In order to facilitate the projection onto simplex constraints, below we consider a non-Euclidean (Banach) space induced by ℓ_1 -norm. In such a space, the Bregman distance between two vectors \mathbf{x} and \mathbf{y} is the KL divergence

$$W(\mathbf{x}, \mathbf{y}) = \sum_{l=1,2,\dots} x_l \ln \left(\frac{x_l}{y_l} \right), \quad (23)$$

and the following proposition can be established.

Proposition 3. *If the classification error $\mu = \max_m \beta_m \Xi_m(\mathbf{p})$ is upper bounded by $\mu \leq \mu_0$, then $\Upsilon(\boldsymbol{\alpha}, \mathbf{p})$ is $(L_1, L_2, L_2, 0)$ -smooth in Banach space induced by ℓ_1 -norm, where*

$$\begin{aligned} L_1 = & \max_{\substack{m=1,\dots,M \\ k=1,\dots,K}} \frac{\beta_m a_m b_m BT G_{k,k}}{D_m \ln 2 \sigma^4} \left(\frac{\mu_0}{\beta_m a_m} \right)^{1+1/b_m} \\ & \times \left[G_{k,k} + \frac{(b_m + 1) BT H_m}{D_m \ln 2} \left(\frac{\mu_0}{\beta_m a_m} \right)^{1/b_m} \right], \end{aligned} \quad (24a)$$

$$L_2 = \max_{m=1, \dots, M} \frac{\beta_m a_m b_m B T H_m}{D_m \ln 2 \sigma^2} \left(\frac{\mu_0}{\beta_m a_m} \right)^{1+1/b_m}, \quad (24b)$$

with $H_m := \left\| \left[\mathbb{I}_{y_m}(1) \times G_{1,1}, \dots, \mathbb{I}_{y_m}(K) \times G_{K,K} \right]^T \right\|_2$.

Proof. See Appendix C. ■

The smoothness result in **Proposition 3** enables us to apply mirror descent (i.e., generalized gradient descent in non-Euclidean space) to \mathbf{p} and mirror ascent to $\boldsymbol{\alpha}$ in the ℓ_1 -space [41]. This leads to the proposed mirror-prox LCPA, which is an iterative algorithm that involves i) a proximal step and ii) an extragradient step. In particular, the mirror-prox LCPA initially chooses a feasible $\mathbf{p} = \mathbf{p}^{[0]} \in \mathcal{P}$ and $\boldsymbol{\alpha} = \boldsymbol{\alpha}^{[0]} \in \mathcal{A}$ (e.g., $\mathbf{p}^{[0]} = P/K \mathbf{1}_K$ and $\boldsymbol{\alpha}^{[0]} = 1/M \mathbf{1}_M$). Denoting the solution at the n^{th} iteration as $(\mathbf{p}^{[n]}, \boldsymbol{\alpha}^{[n]})$, the following equations are used to update the next-round solution [41]:

$$\text{Proximal :} \quad \mathbf{p}^\diamond = \underset{\mathbf{p} \in \mathcal{P}}{\operatorname{argmin}} W(\mathbf{p}, \mathbf{p}^{[n]}) + \eta \mathbf{p}^T \left[\sum_{m=1}^M \alpha_m^{[n]} \beta_m \nabla_{\mathbf{p}} \Xi_m(\mathbf{p}^{[n]}) \right], \quad (25a)$$

$$\boldsymbol{\alpha}^\diamond = \underset{\boldsymbol{\alpha} \in \mathcal{A}}{\operatorname{argmin}} W(\boldsymbol{\alpha}, \boldsymbol{\alpha}^{[n]}) - \eta [\beta_1 \Xi_1(\mathbf{p}^{[n]}), \dots, \beta_M \Xi_M(\mathbf{p}^{[n]})] \boldsymbol{\alpha}. \quad (25b)$$

$$\text{Extragradient :} \quad \mathbf{p}^{[n+1]} = \underset{\mathbf{p} \in \mathcal{P}}{\operatorname{argmin}} W(\mathbf{p}, \mathbf{p}^{[n]}) + \eta \mathbf{p}^T \left[\sum_{m=1}^M \alpha_m^\diamond \beta_m \nabla_{\mathbf{p}} \Xi_m(\mathbf{p}^\diamond) \right], \quad (25c)$$

$$\boldsymbol{\alpha}^{[n+1]} = \underset{\boldsymbol{\alpha} \in \mathcal{A}}{\operatorname{argmin}} W(\boldsymbol{\alpha}, \boldsymbol{\alpha}^{[n]}) - \eta [\beta_1 \Xi_1(\mathbf{p}^\diamond), \dots, \beta_M \Xi_M(\mathbf{p}^\diamond)] \boldsymbol{\alpha}, \quad (25d)$$

where η is the step-size, and the terms inside $[\dots]$ in (25a)–(25d) are obtained from (20a)–(20b). Notice that a small η would lead to slow convergence of the algorithm while a large η would cause the algorithm to diverge. According to [41], η should be chosen inversely proportional to Lipschitz constant L_1 or L_2 derived in **Proposition 3**. In this paper, we set $\eta = 10^3/L_2$ with $\mu_0 = 0.1$, which empirically provides fast convergence of the algorithm.

How Mirror-prox LCPA Works. The major features of the mirror-prox LCPA are summarized as follows:

- The formulas (25a)–(25b) update the variables along their gradient direction, while keeping the updated point $\{\mathbf{p}^\diamond, \boldsymbol{\alpha}^\diamond\}$ close to the current point $\{\mathbf{p}^{[n]}, \boldsymbol{\alpha}^{[n]}\}$. This is achieved via the *proximal operator* that minimizes the distance $W(\mathbf{p}, \mathbf{p}^{[n]})$ (or $W(\boldsymbol{\alpha}, \boldsymbol{\alpha}^{[n]})$) plus a first-order linear function. Moreover, since the KL divergence is the Bregman distance, the update (25a)–(25b) is a Bregman proximal step.

- The signs for updating the upper level variable \mathbf{p} and the lower level variable α are *opposite*, because the upper layer is a minimization problem while the lower layer is a maximization problem.
- The gradients in (25a) and (25c) are computed using $\mathbf{p}^{[n]}$ and \mathbf{p}^\diamond , respectively. By doing so, we can obtain the look-ahead gradient at the intermediate point \mathbf{p}^\diamond for updating $\mathbf{p}^{[n+1]}$. This “look-ahead” feature is called *extragradient*, which is also applied in (25b) and (25d).

Lastly, by putting the Bregman distance W in (23), the function Ξ_m in (13), the gradient in (21), and a proper η into (25a)–(25b), the equations (25a)–(25b) are shown in Appendix D to be equivalent to

$$p_k^\diamond = P p_k^{[n]} \exp \left[-\eta \left(\sum_{m=1}^M \alpha_m^{[n]} \beta_m \nabla_{p_k} \Xi_m(\mathbf{p}^{[n]}) \right) \right] \times \left\{ \sum_{i=1}^K p_i^{[n]} \exp \left[-\eta \left(\sum_{m=1}^M \alpha_m^{[n]} \beta_m \nabla_{p_i} \Xi_m(\mathbf{p}^{[n]}) \right) \right] \right\}^{-1}, \quad \forall k, \quad (26a)$$

$$\alpha_m^\diamond = \alpha_m^{[n]} \exp [\eta \beta_m \Xi_m(\mathbf{p}^{[n]})] \left(\sum_{i=m}^M \alpha_i^{[n]} \exp [\eta \beta_i \Xi_i(\mathbf{p}^{[n]})] \right)^{-1}, \quad \forall m. \quad (26b)$$

Following a similar procedure to Appendix D, the equations (25c)–(25d) can also be reduced to an explicit form.

According to **Proposition 3** and [40], the mirror-prox LCPA algorithm is guaranteed to converge to the optimal solution to P4. But in practice, we can terminate the iterative procedure when the norm $\|\mathbf{p}^{[n]} - \mathbf{p}^{[n-1]}\|_\infty$ is small enough, e.g., $\|\mathbf{p}^{[n]} - \mathbf{p}^{[n-1]}\|_\infty < 10^{-8}$. The entire procedure for computing the solution to P4 using the mirror-prox LCPA is summarized in Fig. 3b. In terms of computational complexity, computing (26a) requires a complexity of $\mathcal{O}(MK)$. Since the number of iterations for the mirror-prox LCPA to converge is $\mathcal{O}(1/\epsilon)$ with ϵ being the target solution accuracy, the total complexity of mirror-prox LCPA would be $\mathcal{O}(MK/\epsilon)$.

C. Accelerated LCPA

For the mirror-prox LCPA method, while the per-iteration complexity is $\mathcal{O}(MK)$, the number of iterations is $\mathcal{O}(1/\epsilon)$ in the worst case, where ϵ is the target solution accuracy. However, it is known that the number of iterations for FOMs could be potentially reduced to $\mathcal{O}(1/\sqrt{\epsilon})$ if the objective function is smooth [43], and the gap between $\mathcal{O}(1/\epsilon)$ and $\mathcal{O}(1/\sqrt{\epsilon})$ is significant [43]–[46]. For example, if ϵ takes a common value of 10^{-4} , then $\mathcal{O}(1/\epsilon)$ is on the order of 10000 iterations but $\mathcal{O}(1/\sqrt{\epsilon})$ is on the order of 100 iterations.

In order to derive a FOM algorithm with $\mathcal{O}(1/\sqrt{\epsilon})$ iterations for the edge machine learning resource allocation problem, we consider a smooth variant of P2, which minimizes the *average* classification error:

$$\text{P5} : \min_{\mathbf{p} \in \mathcal{P}} \frac{1}{M} \sum_{m=1}^M \beta_m \Xi_m(\mathbf{p}), \quad (27)$$

where Ξ_m is defined in (13). In this case, the proposed accelerated gradient learning centric power allocation (accelerated LCPA) solves P5 via the following update at the n^{th} iteration:

$$\mathbf{p}^{[n+1]} = \Pi_{\mathcal{P}} \left[\mathbf{q}^{[n]} - \eta \frac{1}{M} \sum_{m=1}^M \beta_m \nabla_{\mathbf{p}} \Xi_m(\mathbf{q}^{[n]}) \right], \quad (28)$$

where η is the step-size, $\Pi_{\mathcal{P}}(\mathbf{u})$ is the projection of \mathbf{u} onto set \mathcal{P} , and $\mathbf{q}^{[n]}$ is a linear combination of $\mathbf{p}^{[n]}$ and $\mathbf{p}^{[n-1]}$ for acceleration. The detailed procedure for computing η , $\Pi_{\mathcal{P}}(\mathbf{u})$ and $\mathbf{q}^{[n]}$ is as follows.

- To guarantee convergence, the step-size η needs to satisfy [43]:

$$\frac{1}{\eta} \mathbf{I} \succeq \frac{1}{M} \sum_{m=1}^M \beta_m \nabla_{\mathbf{p}}^2 \Xi_m(\mathbf{p}). \quad (29)$$

Since the right hand side is upper bounded as

$$\frac{1}{M} \sum_{m=1}^M \beta_m \nabla_{\mathbf{p}}^2 \Xi_m(\mathbf{p}) \preceq \frac{1}{M} \sum_{m=1}^M \beta_m \times \frac{\sqrt{K} L_1}{\beta_m} \mathbf{I} = \sqrt{K} L_1 \mathbf{I}, \quad (30)$$

where the first inequality is due to part (ii) of **Lemma 1** in Appendix C, the step-size can be set to $\eta \propto 1/(\sqrt{K} L_1)$ (e.g, we use $\eta = 10^3/(\sqrt{K} L_1)$ in the simulation).

- The projection $\Pi_{\mathcal{P}}(\mathbf{u})$ can be computed based on [47, Proposition 2.2]:

$$\Pi_{\mathcal{P}}(\mathbf{u}) = \left(\mathbf{u} - \frac{\sum_{l=1}^{\delta} z_l - P}{\delta} \right)^+, \quad (31)$$

where \mathbf{z} is a permuted version of \mathbf{u} such that $z_1 \geq \dots \geq z_K$ and

$$\delta = \max_{x \in \{1, \dots, K\}} \left\{ x : \frac{\sum_{l=1}^x z_l - P}{x} < z_x \right\}. \quad (32)$$

- Computing the acceleration point $\mathbf{q}^{[n]}$ [45, Sec. 4]:

$$\mathbf{q}^{[n]} = \mathbf{p}^{[n]} + \frac{c^{[n-1]} - 1}{c^{[n]}} (\mathbf{p}^{[n]} - \mathbf{p}^{[n-1]}), \quad (33)$$

where $c^{[n]}$ is a parameter to control the importance of $\mathbf{p}^{[n]} - \mathbf{p}^{[n-1]}$ and is given by

$$c^{[0]} = 1, \quad c^{[n]} = \frac{1}{2} \left(1 + \sqrt{1 + 4(c^{[n-1]})^2} \right). \quad (34)$$

How Accelerated LCPA Works. The idea of accelerated LCPA is that the gradient method is too conservative. Therefore, we need to add some accelerations (the quantity $\mathbf{p}^{[n]} - \mathbf{p}^{[n-1]}$ in (33)) and compute the “look ahead gradient” at the accelerated point $\mathbf{q}^{[n]}$ [43]. However, to guarantee that the acceleration would not be too “confident”, the sequence $c^{[n]}$, which represents how much we trust in the acceleration [44], must be carefully designed as (34). It has been proved in [43]–[45] that $\mathbf{p}^{[n+1]}$ computed using (28)–(34) is guaranteed to converge to the optimal solution to P5 with an iteration complexity $\mathcal{O}(1/\sqrt{\epsilon})$. Since this iteration complexity has touched the lower bound derived for any smooth problem [43, Theorem 2.1.6], the proposed accelerated LCPA is among the fastest FOMs for solving P5. The entire procedure of the accelerated LCPA is summarized in Fig. 3b, and its total complexity is $\mathcal{O}(MK/\sqrt{\epsilon})$.

VI. SIMULATION RESULTS AND DISCUSSIONS

This section provides simulation results to evaluate the performance of the proposed algorithms. It is assumed that the noise power $\sigma^2 = -77$ dBm (corresponding to power spectral density -130 dBm/Hz with 180 kHz bandwidth [27]), which includes thermal noise and receiver noise. The total transmit power at users is set to $P = 13$ dBm (i.e., 20 mW), with the communication bandwidth $B = 180$ kHz. The path loss of the k^{th} user $\rho_k = -90$ dB is adopted [33], and \mathbf{h}_k is generated according to $\mathcal{CN}(\mathbf{0}, \rho_k \mathbf{I}_N)$ [37]. Unless otherwise specified, the time budget $T = 5$ s. Each point in the figures is obtained by averaging over 10 simulation runs, with independent channels in each run. All optimization problems are solved by Matlab R2015b on a desktop with Intel Core i5-4570 CPU at 3.2 GHz and 8 GB RAM. All the classifiers are trained by Python 3.6 on a GPU server with Intel Core i7-6800 CPU at 3.4 GHz and GeForce GTX 1080 GPU.

A. CNN and SVM

For the edge machine learning system, we consider the aforementioned CNN and SVM classifiers with the number of learning models $M = 2$ at the edge: i) Classification of MNIST dataset [28] via CNN; ii) Classification of digits dataset in Scikit-learn [29] via SVM. The data size of each sample is $D_1 = 6276$ bits for the MNIST dataset and $D_2 = 324$ bits for the digits dataset in Scikit-learn. It is assumed that there are $A_1 = 300$ CNN samples and $A_2 = 200$ SVM samples before transmission. The parameters in the two classification error models are obtained by fitting the model (6) to the initial datasets at the edge, and they are given by

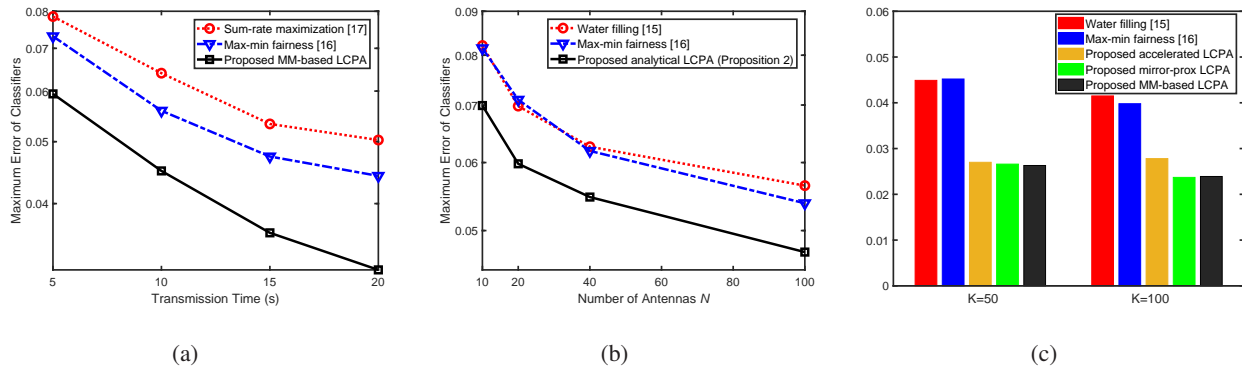


Fig. 4. a) Maximum error of classifiers versus total transmission time T when $K = 4$ and $N = 20$; b) Maximum error of classifiers versus the number of antennas N when $M = K = 2$; c) Maximum classification error versus the number of users K when $N = 100$;

$(a_1, b_1) = (7.3, 0.69)$ for CNN and $(a_2, b_2) = (5.2, 0.72)$ for SVM as in Fig. 2b. Finally, it is assumed that $(\beta_1, \beta_2) = (1, 1.2)$ since the approximation error of SVM in Fig. 2b is larger than that of CNN.

To begin with, the case of $N = 20$ and $K = 4$ with $\mathcal{Y}_1 = \{1\}$ and $\mathcal{Y}_2 = \{2, 3, 4\}$ is simulated. Under the above settings, we compute the collected sample sizes by executing the proposed MM-based LCPA, and the classification error (obtained from the machine learning experiment using the sample sizes from the power allocation algorithms) versus the total transmission time T is shown in Fig. 4a. Besides the proposed MM-based LCPA, we also simulate two benchmark schemes: 1) Max-min fairness scheme [16, Sec. II-C]; 2) Sum-rate maximization scheme [17, Sec. IV]. It can be seen from Fig. 4a that the proposed MM-based LCPA algorithm with $\text{Iter} = 10$ has a significantly smaller classification error compared to other schemes, and the gap concisely quantifies the benefit brought by more training images for CNN under joint communication and learning design. For example, at $T = 20$ in Fig. 4a, the proposed MM-based LCPA collects 2817 MNIST images on average, while the sum-rate maximization and the max-min fairness schemes obtain 1686 images and 1781 images, respectively. Furthermore, if we target at the same learning error, the proposed algorithm saves the transmission time by at least 30% compared to benchmark schemes. This can be seen from Fig. 4a at the target error 4.5%, where the proposed algorithm takes 10 seconds for transmission, but other methods require about 20 seconds. The saved time enables the edge to collect data for other computation offloading tasks [48].

To get more insight into the edge learning system, the case of $K = 2$ with $\mathcal{Y}_1 = \{1\}$ and $\mathcal{Y}_2 = \{2\}$ is simulated, and the classification error versus the number of antennas $N = \{10, 20, 40, 100\}$

TABLE II
COMPARISON OF AVERAGE TRANSMIT POWER IN mW WHEN $N = 10$

User	Analytical LCPA	Water-filling	Max-min fairness
$k = 1$ (for CNN)	19.8476	9.9862	10.0869
$k = 2$ (for SVM)	0.1524	10.0138	9.9131

TABLE III
COMPARISON OF AVERAGE EXECUTION TIME IN SECOND WHEN $N = 100$

Number of Users	MM-based LCPA	Mirror-prox LCPA	Accelerated LCPA	Water-filling	Max-min fairness
$K = 50$	9.8601	0.3655	0.0963	0.0036	0.0036
$K = 100$	18.2496	0.5673	0.1765	0.0044	0.0054

is shown in Fig. 4b. It can be seen from Fig. 4b that the classification error decreases as the number of antennas increases, which demonstrates the advantage of employing massive MIMO in edge machine learning. More importantly, the proposed analytical solution in **Proposition 2** outperforms the water-filling⁴ and max-min fairness schemes even at a relatively small number of antennas $N = 10$. This is achieved by allocating much more power resources to the first user (i.e., user uploading datasets for CNN) as shown in Table II, because training CNN is more difficult than that for SVM. Notice that the performance gain brought by LCPA in Fig. 4b is slightly smaller than that in Fig. 4a, since the ratio $|\mathcal{Y}_1|/|\mathcal{Y}_2|$ is increased. But no matter what value $|\mathcal{Y}_1|$ and $|\mathcal{Y}_2|$ take, the proposed LCPA would always outperform existing algorithms due to its learning centric feature.

To verify the performance and the low complexity nature of the mirror-prox LCPA in Section V-B and the accelerated LCPA in Section V-C when the number of antennas is large, the case of $N = 100$ and $K \in \{50, 100\}$ is simulated, with \mathcal{Y}_1 containing the first $1/5$ users and \mathcal{Y}_2 containing the rest $4/5$ users. The maximum error of classifiers versus the number of users K is shown in Fig. 4c. It can be seen that the proposed mirror-prox LCPA and accelerated LCPA algorithms significantly reduce the classification error compared to the water-filling and max-min fairness schemes, and they achieve performance close to that of the MM-based LCPA. Moreover, the mirror-prox LCPA outperforms the accelerated LCPA, since smoothing approximation is

⁴In the case of large N , sum-rate maximization scheme [17, Sec. IV] would reduce to the iterative water-filling scheme [15], which allocates power according to (17).

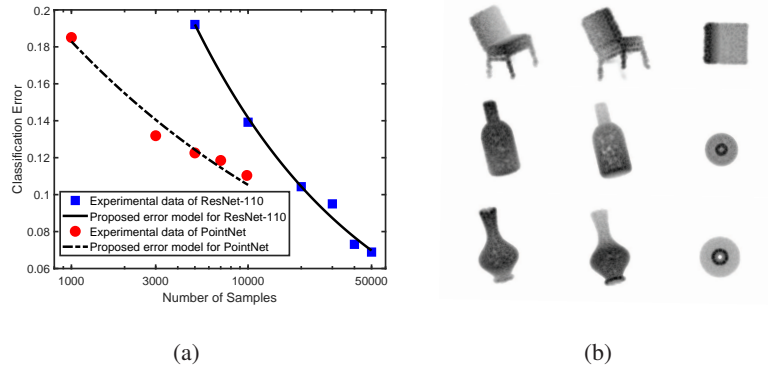


Fig. 5. a) Comparison between the experimental data and the nonlinear classification error model. The parameters in the models are given by $(a_m, b_m) = (8.15, 0.44)$ for ResNet-110 and $(a_m, b_m) = (0.96, 0.24)$ for PointNet; b) Examples of the 3D point clouds in ModelNet40.

involved in the accelerated LCPA. On the other hand, Table III shows the average execution time versus the number of users. Compared with MM-based LCPA, the mirror-prox LCPA saves at least 95% of the computation time for all the simulated values of K , which corroborates the linear complexity derived in Section V-B. Furthermore, the accelerated LCPA is even faster than the mirror-prox LCPA due to the $\mathcal{O}(1/\sqrt{\epsilon})$ convergence rate brought by acceleration, which corroborates the discussions of Section V-C.

B. Deep Neural Networks

To demonstrate the versatility of LCPA under deeper learning models and larger datasets, we train the 110-layer deep residual network (ResNet-110 with 1.7M parameters) [49] using the CIFAR-10 dataset as the input images, with training sample size ranging from 5000 to 50000. The image in the CIFAR-10 dataset has 32×32 pixels (each pixel has 3 bytes representing RGB), and each image sample has a size of $(32 \times 32 \times 3 + 1) \times 8 = 24584$ bits. The training procedure is implemented with a diminishing learning rate and a mini-batch size of 100. After training for 50000 iterations (~ 2.5 hours), we test the trained model on a validation dataset with 10000 unseen samples, and obtain the corresponding classification error. It can be seen from Fig. 5a that the proposed model with $(a_m, b_m) = (8.15, 0.44)$ matches the experiment of ResNet-110 very well.

Moreover, we also consider the PointNet (3.5M parameters), which applies feature transformations and aggregates point features by max pooling [50, Fig. 2] to classify 3D point clouds dataset ModelNet40 (see examples in Fig. 5b). In ModelNet40, there are 12311 CAD models

TABLE IV
MAXIMUM CLASSIFICATION ERROR OF RESNET-110 AND CNN

MM-based LCPA	Sum-rate maximization	Max-min fairness
14.13%	16.79%	16.42%

from 40 object categories, split into 9843 for training and 2468 for testing. Each sample has 2000 points with three single-precision floating-point coordinates, and the data size per sample is $(2000 \times 3 \times 4 + 1) \times 8 = 192008$ bits. After training for 250 epochs (~ 5.5 hours) with a mini-batch of 32, the classification error versus the number of samples is obtained in Fig. 5a, and the proposed classification error model with $(a_m, b_m) = (0.96, 0.24)$ matches the experimental data very well.

Finally, we consider the aforementioned ResNet-110 as task 1 and the CNN in Section II as task 2 at the edge, with $D_1 = 24584$ bits and $D_2 = 6276$ bits. The error rate parameters are given by $(a_1, b_1) = (8.15, 0.44)$ and $(a_2, b_2) = (7.3, 0.69)$. In addition, it is assumed that $(\beta_1, \beta_2) = (1, 1)$, $T = 200$ s, and there is no initial sample at the edge (i.e., $A_1 = A_2 = 0$). We simulate the case of $N = 20$ and $K = 4$ with $\mathcal{Y}_1 = \{1, 2\}$ and $\mathcal{Y}_2 = \{3, 4\}$, and the classification error (obtained from the machine learning experiment using the sample sizes from the power allocation algorithms) is shown in Table IV. It can be seen that the proposed LCPA achieves the smallest classification error, which demonstrates the effectiveness of learning centric algorithm for deep neural networks and large datasets.

VII. CONCLUSIONS

This paper has introduced the LCPA concept to edge machine learning. By adopting an empirical classification error model, learning efficient edge resource allocation has been obtained via the MM-based LCPA algorithm. In the large-scale settings, two fast FOMs have been derived to tackle the curse of high-dimensionality. Simulation results have shown that the proposed LCPA algorithms achieve lower prediction errors than existing power allocation schemes. Furthermore, the proposed fast algorithms significantly reduce the execution time compared with the MM-based LCPA while still achieving satisfactory performance.

APPENDIX A
PROOF OF PROPOSITION 1

To prove part (i), consider the following inequality

$$-\ln \left(\sum_{l=1, l \neq k}^K \frac{G_{k,l} p_l^*}{\sigma^2} + 1 \right) - \frac{\sum_{l=1, l \neq k}^K G_{k,l} p_l / \sigma^2 + 1}{\sum_{l=1, l \neq k}^K G_{k,l} p_l^* / \sigma^2 + 1} + 1 \leq -\ln \left(\sum_{l=1, l \neq k}^K \frac{G_{k,l} p_l}{\sigma^2} + 1 \right), \quad (35)$$

which is obtained from $-\ln(x') - \frac{1}{x'}(x - x') \leq -\ln(x)$ for any (x, x') due to the convexity of $-\ln(x)$. Adding $\ln \left(\sum_{l=1}^K G_{k,l} p_l / \sigma^2 + 1 \right)$ on both sides of (35), we obtain

$$\begin{aligned} & \ln \left(\sum_{l=1}^K \frac{G_{k,l} p_l}{\sigma^2} + 1 \right) - \ln \left(\sum_{l=1, l \neq k}^K \frac{G_{k,l} p_l^*}{\sigma^2} + 1 \right) - \frac{\sum_{l=1, l \neq k}^K G_{k,l} p_l / \sigma^2 + 1}{\sum_{l=1, l \neq k}^K G_{k,l} p_l^* / \sigma^2 + 1} + 1 \\ & \leq \ln \left(\sum_{l=1}^K \frac{G_{k,l} p_l}{\sigma^2} + 1 \right) - \ln \left(\sum_{l=1, l \neq k}^K \frac{G_{k,l} p_l}{\sigma^2} + 1 \right) = \ln \left(1 + \frac{G_{k,k} p_k}{\sum_{l=1, l \neq k}^K G_{k,l} p_l + \sigma^2} \right) \end{aligned} \quad (36)$$

Putting the result of (36) into $\tilde{\Phi}_m(\mathbf{p}|\mathbf{p}^*)$ in (10) and since $a_m x^{-b_m}$ is a decreasing function of x , we immediately prove

$$\tilde{\Phi}_m(\mathbf{p}|\mathbf{p}^*) \geq a_m \left[\sum_{k \in \mathcal{Y}_m} \frac{BT}{D_m \ln 2} \ln \left(1 + \frac{G_{k,k} p_k}{\sum_{l=1, l \neq k}^K G_{k,l} p_l + \sigma^2} \right) + A_m \right]^{-b_m} = \Phi_m(\mathbf{p}). \quad (37)$$

To prove part (ii), we first notice that $\tilde{\Phi}_m(\mathbf{p}|\mathbf{p}^*) = h_m(g_m(\mathbf{p}|\mathbf{p}^*))$ is a composition function of $h_m \circ g_m$, where $h_m(x) = a_m x^{-b_m}$ and

$$\begin{aligned} g_m(\mathbf{p}|\mathbf{p}^*) &= \sum_{k \in \mathcal{Y}_m} \frac{BT}{D_m \ln 2} \left[\ln \left(\sum_{l=1}^K \frac{G_{k,l} p_l}{\sigma^2} + 1 \right) - \ln \left(\sum_{l=1, l \neq k}^K \frac{G_{k,l} p_l^*}{\sigma^2} + 1 \right) \right. \\ & \quad \left. - \frac{\sum_{l=1, l \neq k}^K G_{k,l} p_l / \sigma^2 + 1}{\sum_{l=1, l \neq k}^K G_{k,l} p_l^* / \sigma^2 + 1} + 1 \right] + A_m. \end{aligned} \quad (38)$$

Since $\nabla h_m(x) = -a_m b_m x^{-b_m-1} \leq 0$ and $\nabla^2 h_m(x) = a_m b_m (b_m + 1) x^{-b_m-2} \geq 0$, function $h_m(x)$ is convex and nonincreasing. Adding to the fact that $g_m(\mathbf{p}|\mathbf{p}^*)$ is a concave function of \mathbf{p} , we immediately prove the convexity of $\tilde{\Phi}_m$ using the composition rule [34, Ch. 3, pp. 84].

Finally, to prove $\tilde{\Phi}_m(\mathbf{p}^*|\mathbf{p}^*) = \Phi_m(\mathbf{p}^*)$, we put $\mathbf{p} = \mathbf{p}^*$ into the definition of Φ_m in (10). Then we immediately obtain

$$\begin{aligned} \tilde{\Phi}_m(\mathbf{p}^*|\mathbf{p}^*) &= a_m \left\{ \sum_{k \in \mathcal{Y}_m} \frac{BT}{D_m \ln 2} \left[\ln \left(\sum_{l=1}^K \frac{G_{k,l} p_l^*}{\sigma^2} + 1 \right) - \ln \left(\sum_{l=1, l \neq k}^K \frac{G_{k,l} p_l^*}{\sigma^2} + 1 \right) \right] + A_m \right\}^{-b_m} \\ &= \Phi_m(\mathbf{p}^*). \end{aligned} \quad (39)$$

On the other hand, to prove $\nabla_{\mathbf{p}} \tilde{\Phi}_m(\mathbf{p}^*|\mathbf{p}^*) = \nabla_{\mathbf{p}} \Phi_m(\mathbf{p}^*)$, we first calculate the following derivatives:

$$\begin{aligned} \nabla_{p_j} \tilde{\Phi}_m(\mathbf{p}|\mathbf{p}^*) &= -a_m b_m \left\{ \sum_{k \in \mathcal{Y}_m} \frac{BT}{D_m \ln 2} \left[\ln \left(\sum_{l=1}^K \frac{G_{k,l} p_l}{\sigma^2} + 1 \right) - \ln \left(\sum_{l=1, l \neq k}^K \frac{G_{k,l} p_l^*}{\sigma^2} + 1 \right) \right. \right. \\ &\quad \left. \left. - \frac{\sum_{l=1, l \neq k}^K G_{k,l} p_l / \sigma^2 + 1}{\sum_{l=1, l \neq k}^K G_{k,l} p_l^* / \sigma^2 + 1} + 1 \right] + A_m \right\}^{-b_m - 1} \times \frac{BT}{D_m \ln 2} \\ &\quad \times \left[\sum_{k \in \mathcal{Y}_m} \frac{G_{k,j} / \sigma^2}{\sum_{l=1}^K G_{k,l} p_l / \sigma^2 + 1} - \sum_{k \in \mathcal{Y}_m, k \neq j} \frac{G_{k,j} / \sigma^2}{\sum_{l \neq k}^K G_{k,l} p_l^* / \sigma^2 + 1} \right] \mathbb{I}_{\mathcal{Y}_m}(j), \quad (40a) \end{aligned}$$

$$\begin{aligned} \nabla_{p_j} \Phi_m(\mathbf{p}) &= -a_m b_m \left[\sum_{k \in \mathcal{Y}_m} \frac{BT}{D_m \ln 2} \ln \left(1 + \frac{G_{k,k} p_k}{\sum_{l=1, l \neq k}^K G_{k,l} p_l + \sigma^2} \right) + A_m \right]^{-b_m - 1} \times \frac{BT}{D_m \ln 2} \\ &\quad \times \left[\sum_{k \in \mathcal{Y}_m} \frac{G_{k,j}}{\sum_{l=1}^K G_{k,l} p_l + \sigma^2} - \sum_{k \in \mathcal{Y}_m, k \neq j} \frac{G_{k,j}}{\sum_{l \neq k}^K G_{k,l} p_l + \sigma^2} \right] \mathbb{I}_{\mathcal{Y}_m}(j). \quad (40b) \end{aligned}$$

Then by putting $\mathbf{p} = \mathbf{p}^*$ into (40a)–(40b), the equality $\nabla_{p_j} \tilde{\Phi}_m(\mathbf{p}^*|\mathbf{p}^*) = \nabla_{p_j} \Phi_m(\mathbf{p}^*)$ holds, and the proof for part (iii) is completed.

APPENDIX B

PROOF OF PROPOSITION 2

To prove this proposition, the Lagrangian of P3 is

$$\begin{aligned} L &= \mu + \sum_{k=1}^K \nu_k \left[\beta_k a_k \left(\frac{BT}{D_k} \log_2 \left(1 + \frac{G_{k,k} p_k}{\sigma^2} \right) + A_k \right)^{-b_k} - \mu \right] \\ &\quad + \chi \left(\sum_{k=1}^K p_k - P \right) - \sum_{k=1}^K \theta_k p_k, \quad (41) \end{aligned}$$

where $\{\nu_k, \chi, \theta_k\}$ are non-negative Lagrange multipliers. According to the KKT conditions $\partial L / \partial \mu^* = 0$ and $\partial L / \partial p_k^* = 0$ [34], the optimal $\{\mu^*, p_k^*, \nu_k^*, \chi^*, \theta_k^*\}$ must together satisfy

$$1 - \sum_{k=1}^K \nu_k^* = 0, \quad \chi^* + \nu_k^* \times F_k(p_k^*) = \theta_k^*, \quad \forall k, \quad (42)$$

where

$$F_k(x) = -\beta_k a_k b_k \left[\frac{BT}{D_k} \log_2 \left(1 + \frac{G_{k,k} x}{\sigma^2} \right) + A_k \right]^{-b_k - 1} \times \frac{BT}{D_k \ln 2 (\sigma^2 G_{k,k}^{-1} + x)}, \quad (43)$$

with $x \geq 0$ ($x \neq 0$ if $A_k = 0$). Notice that $F_k(x) < 0$ holds for any $x \geq 0$. Based on the result of (42), it is clear that $\sum_{k=1}^K \frac{\theta_k^* - \chi^*}{F_k(p_k^*)} = 1$. Adding to the fact that $\theta_k^* \geq 0$ and $F_k(p_k^*) < 0$, we must have $\chi^* \neq 0$. Now we will consider two cases.

- $p_k^* = 0$. In this case, $\beta_k a_k u_k^{-b_k} \leq \mu^*$ must hold.
- $p_k^* > 0$. In such a case, based on the complementary slackness condition, we must have $\theta_k^* = 0$. Putting $\theta_k^* = 0$ into (42) and using $\chi^* \neq 0$, $\nu_k^* \neq 0$ holds. Using $\nu_k^* \neq 0$ and the complementary slackness condition, $\beta_k a_k \left(\frac{BT}{D_k} \log_2 \left(1 + \frac{G_{k,k} p_k^*}{\sigma^2} \right) + A_k \right)^{-b_k} = \mu^*$ for all k .

Combining the above two cases gives (16) and the proposition is proved.

APPENDIX C

PROOF OF PROPOSITION 3

To prove this proposition, we need the following lemma for $\nabla_{\mathbf{p}} \Xi_m(\mathbf{p})$.

Lemma 1. *If $\mu \leq \mu_0$, the gradient function $\nabla_{\mathbf{p}} \Xi_m(\mathbf{p})$ satisfies:*

- (i) $\|\nabla_{\mathbf{p}} \Xi_m(\mathbf{p})\|_2 \leq L_2/\beta_m$;
- (ii) $\|\nabla_{\mathbf{p}} \Xi_m(\mathbf{p}) - \nabla_{\mathbf{p}} \Xi_m(\mathbf{p}')\|_\infty \leq L_1/\beta_m \|\mathbf{p} - \mathbf{p}'\|_2$.

Proof. To begin with, the assumption $\mu = \max_m \beta_m \Xi_m(\mathbf{p}) \leq \mu_0$ gives

$$\sum_{k \in \mathcal{Y}_m} \frac{BT}{D_m} \log_2 \left(1 + \frac{G_{k,k} p_k}{\sigma^2} \right) + A_m \geq \left(\frac{\beta_m a_m}{\mu_0} \right)^{1/b_m}, \quad \forall m. \quad (44)$$

Based on (44) and the expression of $\partial \Xi_m / \partial p_j$ in (22), we have

$$\begin{aligned} \left| \frac{\partial \Xi_m}{\partial p_j} \right| &\leq a_m b_m \left(\frac{\beta_m a_m}{\mu_0} \right)^{-1-1/b_m} \frac{BT}{D_m \ln 2 (\sigma^2 G_{j,j}^{-1} + p_j)} \times \mathbb{I}_{\mathcal{Y}_m}(j) \\ &\leq \frac{a_m b_m BT}{D_m \ln 2 \sigma^2} \left(\frac{\mu_0}{\beta_m a_m} \right)^{1+1/b_m} \mathbb{I}_{\mathcal{Y}_m}(j) \times G_{j,j}, \end{aligned} \quad (45)$$

where the second inequality is due to $p_j \geq 0$. Putting the above result into (21), and based on the definition of L_2 in (24b), part (i) is immediately proved.

Next, to prove part (ii), we notice that the derivative in (22) can be rewritten as $\nabla_{p_j} \Xi_m(\mathbf{p}) = h_m(\mathbf{p}) \times g_{m,j}(\mathbf{p})$, where the auxiliary functions

$$h_m(\mathbf{p}) = -a_m b_m \left(\sum_{k \in \mathcal{Y}_m} \frac{BT}{D_m} \log_2 \left(1 + \frac{G_{k,k} p_k}{\sigma^2} \right) + A_m \right)^{-b_m-1}, \quad (46a)$$

$$g_{m,j}(\mathbf{p}) = \frac{BT}{D_m \ln 2 (\sigma^2 G_{j,j}^{-1} + p_j)} \times \mathbb{I}_{\mathcal{Y}_m}(j). \quad (46b)$$

Using the result in (44) and due to $p_j \geq 0$, we have

$$|h_m(\mathbf{p})| \leq a_m b_m \left(\frac{\mu_0}{\beta_m a_m} \right)^{1+1/b_m}, \quad |g_{m,j}(\mathbf{p})| \leq \frac{BT G_{j,j} \mathbb{I}_{\mathcal{Y}_m}(j)}{D_m \ln 2 \sigma^2}. \quad (47)$$

Furthermore, according to Lipschitz conditions [41] of h_m and $g_{m,j}$, they satisfy:

$$\begin{aligned} |h_m(\mathbf{p}) - h_m(\mathbf{p}')| &\leq \sup_{\mathbf{p} \in \mathcal{P}} \|\nabla_{\mathbf{p}} h_m(\mathbf{p})\|_2 \times \|\mathbf{p} - \mathbf{p}'\|_2 \\ &\leq \frac{a_m b_m (b_m + 1) B T H_m}{D_m \ln 2 \sigma^2} \left(\frac{\mu_0}{\beta_m a_m} \right)^{1+2/b_m} \|\mathbf{p} - \mathbf{p}'\|_2, \end{aligned} \quad (48a)$$

$$\begin{aligned} |g_{m,j}(\mathbf{p}) - g_{m,j}(\mathbf{p}')| &\leq \sup_{\mathbf{p} \in \mathcal{P}} \|\nabla_{\mathbf{p}} g_{m,j}(\mathbf{p})\|_2 \times \|\mathbf{p} - \mathbf{p}'\|_2 \\ &\leq \frac{B T G_{j,j}^2 \mathbb{1}_{y_m}(j)}{D_m \ln 2 \sigma^4} \|\mathbf{p} - \mathbf{p}'\|_2. \end{aligned} \quad (48b)$$

As a result, the following inequality is obtained:

$$\begin{aligned} &|\nabla_{p_j} \Xi_m(\mathbf{p}) - \nabla_{p_j} \Xi_m(\mathbf{p}')| \\ &\leq |h_m(\mathbf{p})| |g_{m,j}(\mathbf{p}) - g_{m,j}(\mathbf{p}')| + |h_m(\mathbf{p}) - h_m(\mathbf{p}')| |g_{m,j}(\mathbf{p}')| \\ &\leq \left[a_m b_m \left(\frac{\mu_0}{\beta_m a_m} \right)^{1+1/b_m} \frac{B T G_{j,j}^2}{D_m \ln 2 \sigma^4} + \left(\frac{\mu_0}{\beta_m a_m} \right)^{1+2/b_m} \frac{a_m b_m (b_m + 1) B^2 T^2 G_{j,j} H_m}{D_m^2 \ln^2 2 \sigma^4} \right] \|\mathbf{p} - \mathbf{p}'\|_2 \\ &\leq L_1 / \beta_m \|\mathbf{p} - \mathbf{p}'\|_2, \end{aligned} \quad (49)$$

where the first inequality is due to $|ab+cd| \leq |a||b|+|c||d|$, and the second inequality is obtained from (47) and (48a)-(48b). By taking the maximum of (49) for all j , part (ii) is proved. ■

Based on **Lemma 1**, we are now ready to prove the proposition. In particular, according to [40]–[42], the function $\Upsilon(\boldsymbol{\alpha}, \mathbf{p})$ is $(L_1, L_2, L_2, 0)$ -smooth if and only if

$$\left\| \left[\sum_{m=1}^M \alpha_m \beta_m \nabla_{\mathbf{p}} \Xi_m(\mathbf{p}) \right] - \left[\sum_{m=1}^M \alpha_m \beta_m \nabla_{\mathbf{p}} \Xi_m(\mathbf{p}') \right] \right\|_{\infty} \leq L_1 \|\mathbf{p} - \mathbf{p}'\|_1, \quad (50a)$$

$$\left\| \left[\sum_{m=1}^M \alpha_m \beta_m \nabla_{\mathbf{p}} \Xi_m(\mathbf{p}) \right] - \left[\sum_{m=1}^M \alpha'_m \beta_m \nabla_{\mathbf{p}} \Xi_m(\mathbf{p}) \right] \right\|_{\infty} \leq L_2 \|\boldsymbol{\alpha} - \boldsymbol{\alpha}'\|_1, \quad (50b)$$

$$\left\| [\beta_1 \Xi_1(\mathbf{p}), \dots, \beta_M \Xi_M(\mathbf{p})]^T - [\beta_1 \Xi_1(\mathbf{p}'), \dots, \beta_M \Xi_M(\mathbf{p}')]^T \right\|_{\infty} \leq L_2 \|\mathbf{p} - \mathbf{p}'\|_1, \quad (50c)$$

$$\left\| [\beta_1 \Xi_1(\mathbf{p}), \dots, \beta_M \Xi_M(\mathbf{p})]^T - [\beta_1 \Xi_1(\mathbf{p}), \dots, \beta_M \Xi_M(\mathbf{p})]^T \right\|_{\infty} \leq 0 \times \|\boldsymbol{\alpha} - \boldsymbol{\alpha}'\|_1, \quad (50d)$$

for any $\mathbf{p}, \mathbf{p}' \in \mathcal{P}$ and $\boldsymbol{\alpha}, \boldsymbol{\alpha}' \in \mathcal{A}$. To prove the above inequalities, we need to upper bound the left hand sides of (50a)–(50d) and compare the bounds with the right hand sides of (50a)–(50d).

To this end, the left hand side of (50a) is bounded as

$$\left\| \sum_{m=1}^M \alpha_m \beta_m [\nabla_{\mathbf{p}} \Xi_m(\mathbf{p}) - \nabla_{\mathbf{p}} \Xi_m(\mathbf{p}')] \right\|_{\infty} \leq \sum_{m=1}^M \alpha_m \beta_m \left\| \nabla_{\mathbf{p}} \Xi_m(\mathbf{p}) - \nabla_{\mathbf{p}} \Xi_m(\mathbf{p}') \right\|_{\infty}$$

$$\leq L_1 \|\mathbf{p} - \mathbf{p}'\|_2, \quad (51)$$

where the last inequality is from **Lemma 1**. Further due to $\|\mathbf{p} - \mathbf{p}'\|_2 \leq \|\mathbf{p} - \mathbf{p}'\|_1$, the equation (50a) is proved. On the other hand, the left hand side of (50b) can be upper bounded as

$$\left\| \sum_{m=1}^M (\alpha_m - \alpha'_m) \beta_m \nabla_{\mathbf{p}} \Xi_m(\mathbf{p}) \right\|_{\infty} \leq \sum_{m=1}^M |\alpha_m - \alpha'_m| \left\| \beta_m \nabla_{\mathbf{p}} \Xi_m(\mathbf{p}) \right\|_{\infty} \leq L_2 \|\boldsymbol{\alpha} - \boldsymbol{\alpha}'\|_1, \quad (52)$$

where the last inequality is from **Lemma 1**. In addition, the left hand side of (50c) can be upper bounded as

$$\begin{aligned} & \left\| [\beta_1 \Xi_1(\mathbf{p}) - \beta_1 \Xi_1(\mathbf{p}'), \dots, \beta_M \Xi_M(\mathbf{p}) - \beta_M \Xi_M(\mathbf{p}')]^T \right\|_{\infty} \\ & \leq \max_{m=1, \dots, M} \beta_m \times \sup_{\mathbf{p} \in \mathcal{P}} \|\nabla_{\mathbf{p}} \Xi_m(\mathbf{p})\|_2 \times \|\mathbf{p} - \mathbf{p}'\|_2 \leq L_2 \|\mathbf{p} - \mathbf{p}'\|_1. \end{aligned} \quad (53)$$

Finally, since the left hand side of (50d) is zero, we immediately have (50d) hold.

APPENDIX D

DERIVATION OF (26a) AND (26b)

We will derive (26a), and (26b) can be similarly obtained. In particular, with $W(\mathbf{x}, \mathbf{y})$ in (23) and $\nabla_{\mathbf{p}} \Xi(\mathbf{p})$ in (21), the formula (25a) is rewritten as

$$\min_{\mathbf{p} \in \mathcal{P}} \sum_{k=1}^K p_k \ln \left(\frac{p_k}{p_k^{[n]}} \right) + \eta \mathbf{p}^T \left[\sum_{m=1}^M \alpha_m^{[n]} \beta_m \nabla_{\mathbf{p}} \Xi_m(\mathbf{p}^{[n]}) \right], \quad (54)$$

The Lagrangian of the above problem is

$$L = \sum_{k=1}^K p_k \ln \left(\frac{p_k}{p_k^{[n]}} \right) + \eta \mathbf{p}^T \left[\sum_{m=1}^M \alpha_m^{[n]} \beta_m \nabla_{\mathbf{p}} \Xi_m(\mathbf{p}^{[n]}) \right] + \chi \left(\sum_{k=1}^K p_k - P \right), \quad (55)$$

where $\chi \geq 0$ is the Lagrange multiplier. According to the KKT condition, the optimal \mathbf{p}^* to (54) must satisfy $\nabla_{p_k} L = 0$, leading to

$$p_k^* = p_k^{[n]} \exp \left[-\eta \left(\sum_{m=1}^M \alpha_m^{[n]} \beta_m \nabla_{p_k} \Xi_m(\mathbf{p}^{[n]}) \right) \right] \times \frac{1}{\exp(1 + \chi)}. \quad (56)$$

Combining $\sum_{k=1}^K p_k^* = P$, we obtain (26a).

REFERENCES

- [1] V. Vapnik, *The Nature of Statistical Learning Theory*, Springer, New York, 1998.
- [2] Y. LeCun, Y. Bengio, and G. Hinton, “Deep learning,” *Nature*, vol. 521, pp. 436–444, May 2015.
- [3] M. Stolpe, “The Internet of Things: Opportunities and challenges for distributed data analysis,” *ACM SIGKDD Explorations Newsletter*, vol. 18, no. 1, pp. 15–34, Jun. 2016.
- [4] H. Li, K. Ota, and M. Dong, “Learning IoT in edge: Deep learning for the Internet of Things with edge computing,” *IEEE Network*, vol. 32, no. 1, pp. 96–101, Feb. 2018.
- [5] G. Zhu, D. Liu, Y. Du, C. You, J. Zhang, and K. Huang, “Towards an intelligent edge: Wireless communication meets machine learning,” 2019. [Online]. Available at: <https://arxiv.org/abs/1809.00343>.
- [6] J. Park, S. Samarakoon, M. Bennis, and M. Debbah, “Wireless network intelligence at the edge,” *Proceedings of IEEE*, vol. 107, no. 11, pp. 2204–2239, Nov. 2019.
- [7] Z. Zhou, X. Chen, E. Li, L. Zeng, K. Luo, and J. Zhang, “Edge intelligence: Paving the last mile of artificial intelligence with edge computing,” *Proceedings of IEEE*, vol. 107, no. 8, pp. 1738–1762, Aug. 2019.
- [8] H. B. McMahan, E. Moore, D. Ramage, S. Hampson, and B. Arcas, “Communication-efficient learning of deep networks from decentralized data,” in *Proc. AISTATS*, Fort Lauderdale, Florida, Apr. 2017.
- [9] S. Wang, T. Tuor, T. Salonidis, K. K. Leung, C. Makaya, T. He, and K. Chan, “Adaptive federated learning in resource constrained edge computing systems,” *IEEE J. Sel. Areas Commun.*, vol. 37, no. 6, pp. 1205–1221, Jun. 2019.
- [10] D. Gündüz, P. de Kerret, N. D. Sidiropoulos, D. Gesbert, C. Murthy, and M. van der Schaar, “Machine learning in the air,” 2019. [Online]. Available at: <https://arxiv.org/abs/1904.12385>.
- [11] C. Zhang, P. Patras, and H. Haddadi, “Deep learning in mobile and wireless networking: A survey,” *IEEE Commun. Surveys Tuts.*, vol. 21, no. 3, pp. 2224–2287, Thirdquarter, 2019.
- [12] F. Tariq, M. R. A. Khandaker, K.-K. Wong, M. Imran, M. Bennis, and M. Debbah, “A speculative study on 6G,” 2019. [Online]. Available at: <https://arxiv.org/abs/1902.06700>.
- [13] W. Saad, M. Bennis, and M. Chen, “A vision of 6G wireless systems: Applications, trends, technologies, and open research problems,” *IEEE Network*, to appear in 2019. DOI: 10.1109/MNET.001.1900287.
- [14] K. B. Letaief, W. Chen, Y. Shi, J. Zhang, and Y.-J. A. Zhang, “The roadmap to 6G—AI empowered wireless networks,” *IEEE Communications Magazine*, vol. 57, no. 8, pp. 84–90, Aug. 2019.
- [15] W. Yu, W. Rhee, S. Boyd, and J. M. Cioffi, “Iterative water-filling for Gaussian vector multiple-access channels,” *IEEE Trans. Inf. Theory*, vol. 50, no. 1, pp. 145–152, Jan. 2004.
- [16] M. Schubert and H. Boche, “Solution of the multiuser downlink beamforming problem with individual SINR constraints,” *IEEE Trans. Veh. Technol.*, vol. 53, no. 1, pp. 18–28, Jan. 2004.
- [17] H. Al-Shatri and T. Weber, “Achieving the maximum sum rate using D.C. programming in cellular networks,” *IEEE Trans. Signal Process.*, vol. 60, no. 3, pp. 1331–1341, Mar. 2012.
- [18] A. Beck, A. Nedić, A. Ozdaglar, and M. Teboulle, “An $O(1/\epsilon)$ gradient method for network resource allocation problems,” *IEEE Trans. Control Netw. Syst.*, vol. 1, no. 1, pp. 64–73, Mar. 2014.
- [19] S. Geman, E. Bienenstock, and R. Doursat, “Neural networks and the bias/variance dilemma,” *Neural Comput.*, vol. 4, no. 1, pp. 1–58, 1992.
- [20] P. Domingos, “A unified bias-variance decomposition and its applications,” in *Proc. ICML*, pp. 231–238, 2000.
- [21] M. Johnson, P. Anderson, M. Dras, and M. Steedman, “Predicting classification error on large datasets from smaller pilot data,” in *Proc. ACL*, Melbourne, Australia, Jul. 2018, pp. 450–455.

- [22] P. Kolachina, N. Cancedda, M. Dymetman, and S. Venkatapathy, “Prediction of learning curves in machine translation,” in *Proc. ACL*, Jeju Island, Korea, pp. 22–30, 2012.
- [23] I. Y. Chen, F. D. Johansson, and D. Sontag, “Why is my classifier discriminatory?” in *Proc. NIPS*, Montréal, Canada, 2018, pp. 3543–3554.
- [24] H. S. Seung, H. Sompolinsky, and N. Tishby, “Statistical mechanics of learning from examples,” *Physical Review A*, vol. 45, pp. 6056–6091, Apr. 1992.
- [25] D. Yarowsky, “Unsupervised word sense disambiguation rivaling supervised methods,” in *Proc. ACL*, Stroudsburg, PA, 1995, pp. 189–196.
- [26] I. Radosavovic, P. Dollaf, R. Girshick, G. Gkioxari, and K. He, “Data distillation: Towards omni-supervised learning,” in *Proc. CVPR*, 2018, pp. 4119–4128.
- [27] 3GPP, TS 36.104, “Performance requirements for Narrowband IoT,” Sep. 2018.
- [28] L. Deng, “The MNIST database of handwritten digit images for machine learning research,” *IEEE Signal Process. Mag.*, vol. 29, no. 6, pp. 141–142, Nov. 2012.
- [29] F. Pedregosa, G. Varoquaux, A. Gramfort, *et al.*, “Scikit-learn: Machine learning in Python,” *J. Mach. Learn. Res.*, vol. 12, pp. 2825–2830, Oct. 2011.
- [30] B. R. Marks and G. P. Wright, “A general inner approximation algorithm for nonconvex mathematical programs,” *Operation Research*, vol. 26, no. 4, Jul. 1978.
- [31] T. Lipp and S. Boyd, “Variations and extensions of the convex-concave procedure,” *Optimization and Engineering*, vol. 17, no. 2, pp. 263–287, Jun. 2016.
- [32] Y. Sun, P. Babu, and D. P. Palomar, “Majorization-minimization algorithms in signal processing, communications, and machine learning,” *IEEE Trans. Signal Process.*, vol. 65, no. 3, pp. 794–816, Feb. 2017.
- [33] S. Wang, M. Xia, K. Huang, and Y.-C. Wu, “Wirelessly powered two-way communication with nonlinear energy harvesting model: Rate regions under fixed and mobile relay,” *IEEE Trans. Wireless Commun.*, vol. 16, no. 12, pp. 8190–8204, Dec. 2017.
- [34] S. Boyd and L. Vandenberghe, *Convex Optimization*. Cambridge, U.K.: Cambridge Univ. Press, 2004.
- [35] A. Ben-Tal and A. Nemirovski, *Lectures on Modern Convex Optimization* (MPS/SIAM Series on Optimizations), Philadelphia, PA, USA: SIAM, 2013.
- [36] L. Lu, G. Y. Li, A. L. Swindlehurst, A. Ashikhmin, and R. Zhang, “An overview of massive MIMO: Benefits and challenges,” *IEEE J. Sel. Topics Signal Process.*, vol. 8, no. 5, pp. 742–758, Oct. 2014.
- [37] H. Q. Ngo, E. G. Larsson, and T. L. Marzetta, “Energy and spectral efficiency of very large multiuser MIMO systems,” *IEEE Trans. Commun.*, vol. 61, no. 4, pp. 1436–1449, Apr. 2013.
- [38] L. Liu and W. Yu, “Massive connectivity with massive MIMO Part I: Device activity detection and channel estimation,” *IEEE Trans. Signal Process.*, vol. 66, no. 11, pp. 2933–2946, Jun. 2018.
- [39] K. E. Atkinson, *An Introduction to Numerical Analysis (2nd edition)*, New York: John Wiley and Sons, 1989.
- [40] A. Nemirovski, “Prox-method with rate of convergence $O(1/T)$ for variational inequalities with Lipschitz continuous monotone operators and smooth convex-concave saddle point problems,” *SIAM J. Optimiz.*, vol. 15, no. 1, pp. 229–251, 2004.
- [41] S. Bubeck, “Convex optimization: Algorithms and complexity,” *Foundations and Trends in Machine Learning*, vol. 8, no. 3-4, pp. 231–357, Nov. 2015.
- [42] A. Konar and N. D. Sidiropoulos, “Fast approximation algorithms for a class of non-convex QCQP problems using first-order methods,” *IEEE Trans. Signal Process.*, vol. 65, no. 13, pp. 3494–3509, Jul. 2017.
- [43] Y. Nesterov, *Introductory Lectures on Convex Optimization: A Basic Course*, Applied Optimization. Springer, 2004.

- [44] W. Su, S. Boyd, and E. J. Candes, “A differential equation for modeling Nesterov’s accelerated gradient method: Theory and insights”, *J. Mach. Learn. Res.*, vol. 17, no. 153, pp. 1–43, Sep. 2016.
- [45] A. Beck and M. Teboulle, “A fast iterative shrinkage-thresholding algorithm for linear inverse problems,” *SIAM J. Imaging Sci.*, vol. 2, no. 1, pp. 183–202, Mar. 2009.
- [46] S. Wang, M. Xia, and Y.-C. Wu, “Multicast wirelessly powered network with large number of antennas via first-order method,” *IEEE Trans. Wireless Commun.*, vol. 17, no. 6, pp. 3781–3793, Jun. 2018.
- [47] L. Condat, “Fast projection onto the simplex and the ℓ_1 -ball,” *Math. Program.*, vol. 158, no. 1, pp. 575–585, Jul. 2016.
- [48] S. Yu, B. Dab, Z. Movahedi, R. Langar, and L. Wang, “A socially-aware hybrid computation offloading framework for multi-access edge computing,” *IEEE Trans. Mobile Comput.*, to appear in 2019. DOI: 10.1109/TMC.2019.2908154.
- [49] K. He, X. Zhang, S. Ren, and J. Sun, “Deep residual learning for image recognition,” in *Proc. CVPR*, 2016, Las Vegas, Nevada, pp. 770–778.
- [50] C. R. Qi, H. Su, K. Mo, and L. J. Guibas, “Pointnet: Deep learning on point sets for 3D classification and segmentation,” in *Proc. CVPR*, 2017, Honolulu, Hawaii, pp. 652–660.